

1 **Supplementary information to**

2 **Hydroxyl radical production by air pollutants in epithelial lining fluid governed by**
3 **interconversion and scavenging of reactive oxygen species**

4
5 Steven Lelieveld¹, Jake Wilson¹, Eleni Dovrou¹, Ashmi Mishra¹, Pascale S. J. Lakey², Manabu Shiraiwa²,
6 Ulrich Pöschl¹, Thomas Berkemeier^{1*}

7
8 [1] Multiphase Chemistry Department, Max Planck Institute for Chemistry, 55128 Mainz, Germany

9 [2] Department of Chemistry, University of California, Irvine, Irvine, California 92697, USA

10
11 *Correspondence to: Thomas Berkemeier (t.berkemeier@mpic.de)

12 **Contents of Supporting Information**

13

14 **Additional information**

15 **S1.** ELF antioxidant concentrations

16 **S2.** ELF enzymatic reactions

17 **S3.** OH reactions with unspecified organic matter and estimated OH lifetime in the ELF

18 **S4.** Particulate pollutant concentrations in the ELF

19 **S5.** Gas-phase pollutant concentrations in the ELF

20 **S6.** Acid dissociation

21 **S7.** pH of the ELF

22

23 **Tables**

24 **Table S1.** Chemical reactions

25 **Table S2.** Input parameters to the KM-SUB-ELF model

26 **Table S3.** List of symbols and definitions

27 **Table S4.** Mathematical formulas used to calculate ROS metrics

28 **Table S5.** PM2.5 and transition metal mass fractions

29 **Table S6.** PM2.5 and Secondary Organic Aerosol (SOA) mass fractions

30 **Table S7.** PM2.5 and quinone mass fractions

31

32 **Figures**

33 **Figure S1.** Mass fractions of all redox-active PM2.5 constituents quantified in field data.

34 **Figure S2.** Endpoint, and average ROS concentration, $C_{\Sigma\text{ROS}}$, in the ELF as a function of PM2.5 concentration.

36 **Figure S3.** ROS concentration, $C_{\Sigma\text{ROS}}$, and antioxidant consumption rate as a function of pollutant concentration.

38 **Figure S4.** Gross chemical production of individual ROS in the ELF as a function of the concentration of three distinct pollutants.

40 **Figure S5.** O_3 and NO_2 concentration and saturation point in the ELF as a function of ambient pollutant concentration.

42 **Figure S6.** pH 4 sensitivity study.

43

44 **S1. ELF antioxidant concentrations**

45 Four low molecular weight antioxidants are included in this study, ascorbate (AscH), glutathione (GSH),
46 uric acid (UA) and α -tocopherol (α -Toc).¹ The concentrations of AscH, GSH, and UA in the ELF are 40 μ M,
47 108 μ M, and 200 μ M, respectively.^{2,3} The total α -Toc concentration in the ELF is reported as 0.7 μ M,³
48 however, in the presented study α -Toc is assumed to reside in the surfactant layer of the ELF with a
49 concentration of 200 μ M. It is found that pollutant exposure can lead to a spike in $C_{\Sigma\text{ROS}}$ at pollutant
50 concentrations above 100 $\mu\text{g m}^{-3}$ in the model (Fig. S3a) due to NO₂-driven depletion of ELF antioxidants
51 within the two hours simulation time (Fig. S3b). The reaction mechanism of ROS formation by NO₂ involves
52 formation of GS[·] (R84-85, Tab. S1) and reaction to GSSG[·] (R89), leading to O_{2[·]} production (R91).^{4,5} In the
53 presence of physiological concentrations of UA and AscH, GS[·] is efficiently recycled to GSH (R96, R100)
54 and GSSG[·] formation a minor reaction pathway. However, at low levels of UA and AscH, this O_{2[·]} formation
55 pathway becomes increasingly important.

56

57 Although earlier studies have shown that antioxidants can be consumed in bronchoalveolar lavage fluid
58 after pollutant exposure,⁶ a study using healthy volunteers suggested that the ELF antioxidants may not be
59 fully depleted,⁷ even after exposure to high pollutant concentrations. Kelly et al. found antioxidant
60 concentrations to be non-zero 1.5 hours after exposure to 2 ppm NO₂ stopped, and in some cases
61 exceeded the initial antioxidant concentration several hours after exposure due to antioxidant
62 replenishment.⁷ We are not aware of kinetic data that details the replenishment rates of antioxidants in ELF,
63 but we can assume that they are likely fast enough to prevent full depletion of antioxidants in our two-hour
64 simulations, preventing a spike in $C_{\Sigma\text{ROS}}$ (Fig. S3a). Thus, for simplicity, antioxidant and surfactant
65 concentrations are assumed to stay constant in this study.

66

67 In Fig. S3b, antioxidant consumption rates are shown as a function of NO₂, PM2.5 and O₃ concentration.
68 The dashed line represents the antioxidant consumption rate above which the initial concentration of low
69 molecular mass antioxidants depletes within two hours of pollutant exposure. Note that, without
70 consideration of enzymatic reactions and antioxidant replenishment, it represents a lower limit for healthy
71 individuals.

72

73 **S2. ELF enzymatic reactions**

74 Reactions of the enzymes superoxide dismutase (SOD) and catalase are included in the chemical
75 mechanism (R124, R125, Tab. S1). In our previous work, the SOD-catalyzed reaction of two O_{2[·]} forming
76 H₂O₂ and O₂ was described as a second-order reaction with respect to O_{2[·]} and a rate coefficient of 2.70 \times
77 10⁻¹² cm⁻³ s⁻¹.^{1,8} Dismutation of O_{2[·]} by SOD is a multi-step process, in which one O_{2[·]} is oxidized to O₂,
78 another reduced to H₂O₂, and operates close to the diffusion limit.⁹ Because SOD activity is often reported
79 in terms of a single rate and turnover number, we combine both steps into one effective reaction of SOD

80 and O₂⁻ yielding 0.5 H₂O₂ and 0.5 O₂ (R124, Tab. S1). Note that this reaction is first order with respect to
81 both, O₂⁻ and enzyme.

82 Cantin et al. (1990) showed experimentally that catalase is the most important molecule in H₂O₂ defense
83 of the ELF, exceeding the glutathione peroxidase concentration by nearly two orders of magnitude.¹⁰ The
84 reaction between catalase and H₂O₂ is a two-step reaction in which a molecule of H₂O₂ reacts with catalase
85 to form an enzyme-substrate complex, which then further reacts with another molecule of H₂O₂ to release
86 H₂O and O₂. Because catalase activity is often reported in terms of a single rate and turnover number, we
87 combine both steps into one effective reaction of catalase and H₂O₂, yielding 0.5 H₂O and 0.5 O₂ (R125,
88 Tab. S1).¹¹

89 The catalytic activity of a particular enzyme in biological samples is often reported using the enzyme unit
90 (U) per sample volume or mass. One U is defined as the amount of enzyme needed to catalyze one
91 micromole of substrate per minute. The catalytic activity of a biological sample is generally determined by
92 monitoring substrate decomposition in excess of substrate. Under these conditions, catalytic activity is
93 maximal and a first order dependence exists between the velocity of the enzymatic reaction (v_{max} , in U mL⁻¹)
94 and the enzyme concentration (Eq. S1).¹² The proportionality factor is the turnover number k_{cat} ,
95 sometimes referred to as catalytic constant, and can be used to infer enzyme concentrations.¹³

$$[\text{Enzyme}] = \frac{v_{max}}{k_{cat}} \quad (\text{Eq. S1})$$

96

97 For SOD, k_{cat} is reported to range between 10⁵ – 10⁶ s⁻¹.^{9,14} The activity of SOD in ELF was measured as
98 36.8 ± 2.0 U mL⁻¹,¹⁰ which translates to an enzyme concentration of SOD of 0.58 – 6.5 nM using Eq. S1.
99 Note that, the enzymatic reactions in this study do not occur in excess of substrate. Thus, a second-order
100 rate coefficient for the reaction of SOD with O₂⁻ of 2.65 × 10⁻¹² cm³ s⁻¹ is used in the chemical mechanism
101 (k_{R124}, Tab. S1).^{15,16}

102 Catalase activity in ELF has been estimated to be 3.7 ± 0.6 U mL⁻¹ and for k_{cat} , values in the range of 3 ×
103 10⁶ and 4 × 10⁷ s⁻¹ can be found.^{10,13} From these numbers, we derive a concentration of catalase of 1.3 –
104 24 pM. Second-order rate coefficients for catalase have been measured in the range of 1.6 × 10⁻¹⁴ – 1.6 ×
105 10⁻¹³ cm³ s⁻¹. For this study, we use a rate coefficient of 3.2 × 10⁻¹⁴ cm³ s⁻¹ (k_{R125}, Tab. S1).^{11,17}

106 Given the broad reported ranges of v_{max} and k_{cat} , and the difficulty of sampling ELF, we acknowledge that
107 there is large uncertainty associated with the concentrations of SOD and catalase in the ELF. Therefore,
108 we restrict the determination of enzyme concentration to order of magnitude estimations and use 1 nM for
109 SOD and 5 pM for catalase in this study.

110 Note that the presence of PM may decrease the activity of antioxidant enzymes, as shown for SOD
111 previously.¹⁸ At the high PM concentrations for which these effects were observed, however, antioxidant

112 enzymes contribute only marginally to overall ROS scavenging and interconversion in the model (Figs.
113 4b,d). Thus, enzyme inhibition by PM2.5 requires further investigation in future experimental and modelling
114 studies to clarify whether enzyme inhibition promotes the shift to the PM2.5-dominated kinetic regime of
115 ROS conversion.

116

117 **S3. Unspecific reaction of OH radicals with organic matter and estimated OH lifetime in the** 118 **ELF**

119 OH reacts with nearly all matter present in the ELF with a rate coefficient approaching diffusion limitation.¹⁹
120 Because of this unspecific reactivity, effective scavenging of OH radicals, e.g. through lung antioxidants, is
121 not possible.^{19,20} As an estimate, we assume that the amount of protein in the ELF corresponds to the total
122 amount of dissolved organic matter. The protein mass in the ELF amounts to approximately 10 mg per mL
123 lung fluid.³ Using an average molecular weight of ~125 g mole⁻¹ of a single amino acid, the total amino acid
124 concentration in the ELF can be estimated to ~80 mmol L⁻¹. A second-order reaction of amino acids with
125 OH is included, using a reaction rate coefficient on the order of 1.66×10^{-12} cm⁻³ s⁻¹ (R122, Tab. S1).²¹
126 Because proteins are folded, not all amino acids will be surface exposed, and thus accessible reaction
127 partners for OH. In general, spherical proteins have fewer surface exposed amino acids due to a smaller
128 surface-to-volume ratio, while elongated, cuboid or conical proteins have more surface exposed amino
129 acids. Furthermore, the surface exposure of amino acids depends on the physical properties, e.g. the
130 polarity of the respective amino acid.²² Therefore, as an order of magnitude estimation, we assume that
131 50% of all amino acids are surface exposed in the ELF, yielding an effective amino acid concentration of
132 ~40 mmol L⁻¹ and, in turn, a lifetime of OH with respect to reaction with dissolved organic matter of $2.5 \times$
133 10^{-8} s.

134

135 Pryor estimated the lifetime of OH in a cell to 10^{-9} s, assuming a rate coefficient of 1×10^9 M⁻¹ s⁻¹ (equivalent
136 to 1.66×10^{-12} cm⁻³ s⁻¹) and an effective organic matter concentration of 1 mol L⁻¹.²¹ From comparing the
137 ELF protein mass of ~10 mg mL⁻¹ to the cellular protein mass of ~250 mg mL⁻¹, we infer that the ELF must
138 be about ~25 times more dilute compared to a cell with respect to dissolved organic matter.^{2,23,24} Multiplying
139 Pryor's OH lifetime in cells with this dilution factor yields an estimate for the OH lifetime in ELF of $\sim 2.5 \times$
140 10^{-8} s, which is identical to the estimate above and consolidates our description of OH reactivity.

141

142 We find that inclusion of this second-order loss reaction of OH results in a decrease of momentary OH
143 concentrations by one order of magnitude compared to our earlier calculations (Fig. 2a).¹ This finding
144 suggests that OH will react unspecifically with organic matter and only secondarily with antioxidants (7%)
145 in the ELF. Due to the fast reaction of OH, spatial gradients of reactants could play a role in OH fate, e.g.
146 through local depletion of antioxidants around a dissolving particle or inhomogeneous distribution of organic
147 matter and PM2.5 constituents in the ELF. However, for the calculations in this study, starting
148 concentrations of antioxidants and organic matter were homogeneous across the bulk ELF.

149

150 **S4. Particulate pollutant concentrations in the ELF**151 The ELF concentrations of redox-active PM2.5 constituents, $C_{ELF,Y}$, with Y standing for copper, iron, SOA,
152 or quinones, are calculated using Eq. S2.¹

153

$$C_Y = \frac{C_{gas,PM2.5} \times VR \times t_{acc} \times d_{PM2.5} \times MF_Y \times SF_Y}{M_Y \times V_{ELF}} \quad (\text{Eq. S2})$$

154

155 Inhaled particles can reside in the ELF for several hours.²⁵ For this study, we assume a residence time of
 156 PM2.5 of 2 hours and use this as accumulation time of inhaled particles (t_{acc}) and simulation time (t_{sim}) to
 157 mimic a pseudo steady-state of ROS concentrations that would be achieved through continuous inhalation,
 158 in line with our previous studies.¹ It should be noted that there is some uncertainty regarding the residence
 159 time of PM2.5 in the ELF, with estimates on PM2.5 clearance also exceeding 2 hours.²⁶ As lung ventilation
 160 rate, VR, $1.5 \text{ m}^3 \text{ h}^{-1}$ is used, and the PM2.5 deposition fraction in the ELF, $d_{PM2.5}$, is assumed to be 0.45.^{1,27}
 161 The total ELF volume, V_{ELF} , is set to 20 mL.^{1,28} This study only includes copper and iron as transition metals,
 162 because these are the only two that have been shown to significantly produce ROS in surrogate ELF
 163 (sELF).^{29,30} The fractional solubilities, SF_Y , of copper and iron ions were discussed and tested extensively
 164 in our previous study, including the effects of varying trace metal solubilities.¹ In line with the main results
 165 of our previous study, the fractional solubilities of copper and iron ions are set to 0.4, 0.1, respectively.¹
 166 Due to the relatively small concentration of iron ions and the large concentration of potential organic ligands,
 167 iron ions are expected not to precipitate in the ELF.³¹ For the organic fraction in PM2.5, full solubility is
 168 assumed. Mass fractions (MF) of redox-active PM2.5 constituents are derived from field observations and
 169 tabulated in Tables S4-S6. Not all references in Tables S4 and S6 include PM2.5 concentrations. In such
 170 cases, PM2.5 concentrations are estimated based on similar geographical locations and indicated with an
 171 asterisk. Additionally, secondary organic aerosol (SOA) forms ROS and is included in the model.³²⁻³⁴
 172 However, because the exact mechanism of ROS formation by SOA in the ELF, first order formation rates
 173 of H_2O_2 and OH by SOA were parameterized based on experimental observations.^{1,32,33} Quinones in PM2.5
 174 are included in this study as previously described.¹ Three quinones are included that were shown to form
 175 ROS in sELF, phenanthrenequinone (PQN), 1,2-naphthoquinone (1,2-NQN), and 1,4-naphthoquinone (1,4-
 176 NQN) in a molar ratio of 2:1:1.²⁹

177

178 **S5. Gas-phase pollutant concentrations in the ELF**

179 Exposure to gas-phase oxidants, O_3 and NO_2 is quantified in the model using a simplified breathing
 180 mechanism. In our previous study, it was assumed that the concentrations of these gas-phase oxidants in
 181 the lung were equal to their respective ambient concentrations. However, because of the reactivity of these
 182 oxidants, we find that lung gas-phase concentrations of these oxidants are depressed and limited by supply
 183 from inhalation of ambient air. In order to get accurate estimates for the amount of gas-phase oxidants

184 transferred to the surfactant layer and ELF, an average lung volume of four L, an average breath volume
185 of 1.5 L and an average duration of a breath of 3.6 s are used to compute mass fluxes into and out of the
186 lung (Table S2). Application of this simplified breathing mechanism results in a significant decrease in the
187 amount of gaseous oxidants in the surfactant layer and ELF. Therefore, neither O₃, nor NO₂ are saturated
188 in ELF with respect to their ambient concentrations in this study (Fig. S5).

189

190 **S6. Acid dissociation**

191 In this study, corresponding acid/base-pairs are treated as a single species in the numerical computation
192 of ordinary differential equations (ODE). This effectively reduces the stiffness of the ODE system and
193 applies to glutathione (GSH/GS⁻), superoxide radicals (HO₂/O₂⁻) and peroxy nitrous acid (ONOOH/ONOO⁻).
194 Instead of treating each species explicitly with separate differential equations and explicit protonation and
195 deprotonation reactions, the pKa of these species was used to calculate the acid/base-ratio at the pH of
196 the ELF (Table S2). Then, if a reaction requires only one of the two species to react, the rate of that reaction
197 was multiplied with the inferred fraction of the reacting species.

198

199 **S7. pH of the ELF**

200 Following estimations by Holma (1985, 1989), the pH of the ELF was assumed to stay constant upon air
201 pollutant exposure.^{35,36} In diseased individuals such as asthmatics³⁷, chronic obstructive pulmonary
202 disease,³⁸ or cystic fibrosis patients³⁹ the pH of the ELF may be decreased. Figure S6 shows the ROS
203 concentration, production, interconversion and transition metal valence state at pH 7 and pH 4 as a function
204 of PM2.5 concentration. Panel a shows that C_{ΣROS} displays a very similar behavior at pH 4 and pH 7. C_{O₂}
205 and C_{HO₂} are slightly increased at low PM2.5 concentrations, but depressed at elevated PM2.5
206 concentrations (panel b). This reduction is due to a higher rate of Fe²⁺-mediated interconversion of HO₂
207 and O₂⁻ to H₂O₂ (Table S1, R38 and R39), which in turn is due to a higher Fe²⁺/Fe³⁺ ratio (panel c). The
208 Cu⁺/Cu²⁺ ratio shows the opposite trend at reduced pH (panel j).

209 Panel e shows that at pH 4, N_{ΣROS} is marginally reduced compared to pH 7. In panel f, N_{ΣROS} is broken
210 down to its components. P_{O₂}⁻ is slightly reduced due to decreased Cu⁺-dependent O₂⁻ formation (Table S1,
211 R54). P_{OH} is slightly increased due to the higher Fe²⁺/Fe³⁺ ratio and the according increase in the Fenton
212 reaction (Table S1, R40).

213 Panel g shows that C_{F_{O₂}→H₂O₂} is slightly decreased at low PM2.5 concentration and slightly increased at
214 higher PM2.5 concentrations compared to pH 7. Panel h shows that C_{F_{H₂O₂}→OH} is mostly unaffected by a
215 change in pH. The reduction in N_{ΣROS} (panel e) paired with the increase in P_{OH} (panel f) at higher PM2.5
216 concentrations results in a larger OH fraction (panel i) and a larger increase in OH dose (panel j) at pH 4.

217 Reduced pH in the ELF may additionally lead to a reduction in antioxidant enzyme activity,¹⁷ increased
218 transition metal solubility,⁴⁰ and increased OH yield from the Fenton reaction.^{41,42} These effects are not
219 included in the presented study, and are expected to all reduce ROS buffering and promote the PM2.5-

220 controlled OH radical production regime, which may exacerbate oxidative stress. Furthermore, in the
221 presented study SOA produces H₂O₂ and OH,^{32,33} which at lower pH may increasingly shift towards only
222 H₂O₂ production, without OH getting formed.^{43,44} However, a thorough investigation of pH effects is beyond
223 the scope of the presented study and warrants future investigations.

224 **References**

- 225 (1) Lakey, P. S. J.; Berkemeier, T.; Tong, H.; Arangio, A. M.; Lucas, K.; Pöschl, U.; Shiraiwa, M.
226 Chemical Exposure-Response Relationship between Air Pollutants and Reactive Oxygen Species
227 in the Human Respiratory Tract. *Sci. Rep.* **2016**, *6* (1), 32916.
228 <https://doi.org/10.1038/srep32916>.
- 229 (2) Mudway, I. S.; Kelly, F. J. Ozone and the Lung: A Sensitive Issue. *Mol. Aspects Med.* **2000**, *21* (1–
230 2), 1–48. [https://doi.org/10.1016/S0098-2997\(00\)00003-0](https://doi.org/10.1016/S0098-2997(00)00003-0).
- 231 (3) van der Vliet, A.; O'Neill, C. A.; Cross, C. E.; Koostra, J. M.; Volz, W. G.; Halliwell, B.; Louie, S.
232 Determination of Low-Molecular-Mass Antioxidant Concentrations in Human Respiratory Tract
233 Lining Fluids. *Am. J. Physiol.-Lung Cell. Mol. Physiol.* **1999**, *276* (2), L289–L296.
234 <https://doi.org/10.1152/ajplung.1999.276.2.L289>.
- 235 (4) Kirsch, M.; Lehnig, M.; Korth, H.-G.; Sustmann, R.; de Groot, H. Inhibition of Peroxynitrite-
236 Induced Nitration of Tyrosine by Glutathione in the Presence of Carbon Dioxide through Both
237 Radical Repair and Peroxynitrate Formation. *Chem. Eur. J.* **2001**, *7* (15), 3313–3320.
238 [https://doi.org/10.1002/1521-3765\(20010803\)7:15<3313::aid-chem3313>3.0.co;2-7](https://doi.org/10.1002/1521-3765(20010803)7:15<3313::aid-chem3313>3.0.co;2-7).
- 239 (5) Wardman, P.; Sonntag, C. [3] Kinetic factors that control the fate of thiyl radicals in cells. In
240 *Methods in Enzymology*; Elsevier: gr, 1995; Vol. 251, pp 31–45. [https://doi.org/10.1016/0076-6879\(95\)51108-3](https://doi.org/10.1016/0076-6879(95)51108-3).
- 242 (6) Kelly, F. J.; Tetley, T. D. Nitrogen Dioxide Depletes Uric Acid and Ascorbic Acid but Not
243 Glutathione from Lung Lining Fluid. *Biochem. J.* **1997**, *325* (1), 95–99.
244 <https://doi.org/10.1042/bj3250095>.
- 245 (7) Kelly, F. J.; Blomberg, A.; Frew, A.; Holgate, S. T.; Sandstrom, T. Antioxidant Kinetics in Lung
246 Lavage Fluid Following Exposure of Humans to Nitrogen Dioxide. *Am. J. Respir. Crit. Care Med.*
247 **1996**, *154* (6), 1700–1705. <https://doi.org/10.1164/ajrccm.154.6.8970358>.
- 248 (8) Kohen, R.; Nyska, A. Invited Review: Oxidation of Biological Systems: Oxidative Stress
249 Phenomena, Antioxidants, Redox Reactions, and Methods for Their Quantification. *Toxicol.*
250 *Pathol.* **2002**, *30* (6), 620–650. <https://doi.org/10.1080/01926230290166724>.
- 251 (9) Fee, J. A.; Bull, C. Steady-State Kinetic Studies of Superoxide Dismutases. Saturative Behavior of
252 the Copper- and Zinc-Containing Protein. *J. Biol. Chem.* **1986**, *261* (28), 13000–13005.
253 [https://doi.org/10.1016/S0021-9258\(18\)69261-0](https://doi.org/10.1016/S0021-9258(18)69261-0).
- 254 (10) Cantin, A. M.; Fells, G. A.; Hubbard, R. C.; Crystal, R. G. Antioxidant Macromolecules in the
255 Epithelial Lining Fluid of the Normal Human Lower Respiratory Tract. *J. Clin. Invest.* **1990**, *86* (3),
256 962–971. <https://doi.org/10.1172/JCI114798>.
- 257 (11) Aebi, H. [13] Catalase in Vitro. *Methods Enzymol.* **1984**, *105*, 121–126.
- 258 (12) Bisswanger, H. *Practical Enzymology*; John Wiley & Sons, 2019.
- 259 (13) Smejkal, G. B.; Kakumanu, S. Enzymes and Their Turnover Numbers. *Expert Rev. Proteomics*
260 **2019**, *16* (7), 543–544. <https://doi.org/10.1080/14789450.2019.1630275>.
- 261 (14) Bar-Even, A.; Noor, E.; Savir, Y.; Liebermeister, W.; Davidi, D.; Tawfik, D. S.; Milo, R. The
262 Moderately Efficient Enzyme: Evolutionary and Physicochemical Trends Shaping Enzyme
263 Parameters. *Biochemistry* **2011**, *50* (21), 4402–4410. <https://doi.org/10.1021/bi2002289>.
- 264 (15) Forman, H. J.; Fridovich, I. Superoxide Dismutase: A Comparison of Rate Constants. *Arch.*
265 *Biochem. Biophys.* **1973**, *158* (1), 396–400. [https://doi.org/10.1016/0003-9861\(73\)90636-X](https://doi.org/10.1016/0003-9861(73)90636-X).
- 266 (16) Fridovich, I. Superoxide Dismutases. *Annu. Rev. Biochem.* **1975**, *44* (1), 147–159.
- 267 (17) Jones, P.; Suggett, A. The Catalase–Hydrogen Peroxide System. Kinetics of Catalatic Action at
268 High Substrate Concentrations. *Biochem. J.* **1968**, *110* (4), 617–620.
269 <https://doi.org/10.1042/bj1100617>.

- 270 (18) Hatzis, C.; Godleski, J. J.; González-Flecha, B.; Wolfson, J. M.; Koutrakis, P. Ambient Particulate
271 Matter Exhibits Direct Inhibitory Effects on Oxidative Stress Enzymes. *Environ. Sci. Technol.*
272 **2006**, *40* (8), 2805–2811. <https://doi.org/10.1021/es0518732>.
- 273 (19) Forman, H. J.; Davies, K. J. A.; Ursini, F. How Do Nutritional Antioxidants Really Work:
274 Nucleophilic Tone and Para-Hormesis versus Free Radical Scavenging in Vivo. *Free Radic. Biol.
275 Med.* **2014**, *66*, 24–35. <https://doi.org/10.1016/j.freeradbiomed.2013.05.045>.
- 276 (20) Sies, H.; Berndt, C.; Jones, D. P. Oxidative Stress. *Annu. Rev. Biochem.* **2017**, *86*, 715–748.
277 <https://doi.org/10.1146/annurev-biochem-061516-045037>.
- 278 (21) Pryor, W. A. Oxy-Radicals and Related Species: Their Formation, Lifetimes, and Reactions. *Annu.
279 Rev. Physiol.* **1986**, *48* (1), 657–667.
- 280 (22) Holbrook, S. R.; Muskal, S. M.; Kim, S.-H. Predicting Surface Exposure of Amino Acids from
281 Protein Sequence. *Protein Eng. Des. Sel.* **1990**, *3* (8), 659–665.
282 <https://doi.org/10.1093/protein/3.8.659>.
- 283 (23) Milo, R. What Is the Total Number of Protein Molecules per Cell Volume? A Call to Rethink Some
284 Published Values. *BioEssays* **2013**, *35* (12), 1050–1055.
285 <https://doi.org/10.1002/bies.201300066>.
- 286 (24) Brown, G. C. Total Cell Protein Concentration as an Evolutionary Constraint on the Metabolic
287 Control Distribution in Cells. *J. Theor. Biol.* **1991**, *153* (2), 195–203.
288 [https://doi.org/10.1016/S0022-5193\(05\)80422-9](https://doi.org/10.1016/S0022-5193(05)80422-9).
- 289 (25) Ghio, A. J.; Richards, J. H.; Dittrich, K. L.; Samet, J. M. Metal Storage and Transport Proteins
290 Increase After Exposure of the Rat Lung to an Air Pollution Particle. *Toxicol. Pathol.* **1998**, *26* (3),
291 388–394. <https://doi.org/10.1177/019262339802600313>.
- 292 (26) Lippmann, M.; Yeates, D. B.; Albert, R. E. Deposition, Retention, and Clearance of Inhaled
293 Particles. *Occup. Environ. Med.* **1980**, *37* (4), 337–362. <https://doi.org/10.1136/oem.37.4.337>.
- 294 (27) Sarangapani, R. The Role of Dispersion in Particle Deposition in Human Airways. *Toxicol. Sci.*
295 **2000**, *54* (1), 229–236. <https://doi.org/10.1093/toxsci/54.1.229>.
- 296 (28) Walters, D. V. Lung Lining Liquid – The Hidden Depths. *Neonatology* **2002**, *81* (1), 2–5.
297 <https://doi.org/10.1159/000056764>.
- 298 (29) Charrier, J. G.; McFall, A. S.; Richards-Henderson, N. K.; Anastasio, C. Hydrogen Peroxide
299 Formation in a Surrogate Lung Fluid by Transition Metals and Quinones Present in Particulate
300 Matter. *Environ. Sci. Technol.* **2014**, *48* (12), 7010–7017. <https://doi.org/10.1021/es501011w>.
- 301 (30) Charrier, J. G.; Anastasio, C. Impacts of Antioxidants on Hydroxyl Radical Production from
302 Individual and Mixed Transition Metals in a Surrogate Lung Fluid. *Atmos. Environ.* **2011**, *45* (40),
303 7555–7562. <https://doi.org/10.1016/j.atmosenv.2010.12.021>.
- 304 (31) Gonzalez, D. H.; Diaz, D. A.; Baumann, J. P.; Ghio, A. J.; Paulson, S. E. Effects of Albumin,
305 Transferrin and Humic-like Substances on Iron-Mediated OH Radical Formation in Human Lung
306 Fluids. *Free Radic. Biol. Med.* **2021**, *165*, 79–87.
307 <https://doi.org/10.1016/j.freeradbiomed.2021.01.021>.
- 308 (32) Wang, Y.; Kim, H.; Paulson, S. E. Hydrogen Peroxide Generation from α - and β -Pinene and
309 Toluene Secondary Organic Aerosols. *Atmos. Environ.* **2011**, *45* (18), 3149–3156.
310 <https://doi.org/10.1016/j.atmosenv.2011.02.060>.
- 311 (33) Tong, H.; Arangio, A. M.; Lakey, P. S. J.; Berkemeier, T.; Liu, F.; Kampf, C. J.; Brune, W. H.; Pöschl,
312 U.; Shiraiwa, M. Hydroxyl Radicals from Secondary Organic Aerosol Decomposition in Water.
313 *Atmospheric Chem. Phys.* **2016**, *16* (3), 1761–1771. <https://doi.org/10.5194/acp-16-1761-2016>.
- 314 (34) Tong, H.; Lakey, P. S. J.; Arangio, A. M.; Socorro, J.; Kampf, C. J.; Berkemeier, T.; Brune, W. H.;
315 Pöschl, U.; Shiraiwa, M. Reactive Oxygen Species Formed in Aqueous Mixtures of Secondary
316 Organic Aerosols and Mineral Dust Influencing Cloud Chemistry and Public Health in the
317 Anthropocene. *Faraday Discuss.* **2017**, *200*, 251–270. <https://doi.org/10.1039/C7FD00023E>.

- 318 (35) Holma, B. Influence of Buffer Capacity and PH-Dependent Rheological Properties of Respiratory
319 Mucus on Health Effects Due to Acidic Pollution. *Sci. Total Environ.* **1985**, *41* (2), 101–123.
320 [https://doi.org/10.1016/0048-9697\(85\)90181-0](https://doi.org/10.1016/0048-9697(85)90181-0).
- 321 (36) Holma, B. Effects of Inhaled Acids on Airway Mucus and Its Consequences for Health. *Env.*
322 *Health Perspect* **1989**, No. 79, 109–113.
- 323 (37) Hunt, J. F.; Fang, K.; Malik, R.; Snyder, A.; Malhotra, N.; Platts-Mills, T. A. E.; Gaston, B.
324 Endogenous Airway Acidification: Implications for Asthma Pathophysiology. *Am. J. Respir. Crit.*
325 *Care Med.* **2000**, *161* (3), 694–699. <https://doi.org/10.1164/ajrccm.161.3.9911005>.
- 326 (38) Ricciardolo, F. L. M.; Gaston, B.; Hunt, J. Acid Stress in the Pathology of Asthma. *J. Allergy Clin.*
327 *Immunol.* **2004**, *113* (4), 610–619. <https://doi.org/10.1016/j.jaci.2003.12.034>.
- 328 (39) Tate, S.; MacGregor, G.; Davis, M.; Innes, J.; Greening, A. Airways in Cystic Fibrosis Are Acidified:
329 Detection by Exhaled Breath Condensate. *Thorax* **2002**, *57* (11), 926–929.
- 330 (40) Fang, T.; Guo, H.; Zeng, L.; Verma, V.; Nenes, A.; Weber, R. J. Highly Acidic Ambient Particles,
331 Soluble Metals, and Oxidative Potential: A Link between Sulfate and Aerosol Toxicity. *Environ.*
332 *Sci. Technol.* **2017**, *51* (5), 2611–2620. <https://doi.org/10.1021/acs.est.6b06151>.
- 333 (41) Hug, S. J.; Leupin, O. Iron-Catalyzed Oxidation of Arsenic(III) by Oxygen and by Hydrogen
334 Peroxide: PH-Dependent Formation of Oxidants in the Fenton Reaction. *Environ. Sci. Technol.*
335 **2003**, *37* (12), 2734–2742. <https://doi.org/10.1021/es026208x>.
- 336 (42) Bataineh, H.; Pestovsky, O.; Bakac, A. PH-Induced Mechanistic Changeover from Hydroxyl
337 Radicals to Iron(Iv) in the Fenton Reaction. *Chem. Sci.* **2012**, *3* (5), 1594.
338 <https://doi.org/10.1039/c2sc20099f>.
- 339 (43) Qiu, J.; Tonokura, K.; Enami, S. Proton-Catalyzed Decomposition of α -Hydroxyalkyl-
340 Hydroperoxides in Water. *Environ. Sci. Technol.* **2020**, *54* (17), 10561–10569.
341 <https://doi.org/10.1021/acs.est.0c03438>.
- 342 (44) Enami, S. Fates of Organic Hydroperoxides in Atmospheric Condensed Phases. *J. Phys. Chem. A*
343 **2021**, *125* (21), 4513–4523. <https://doi.org/10.1021/acs.jpca.1c01513>.
- 344 (45) Saunders, S. M.; Jenkin, M. E.; Derwent, R. G.; Pilling, M. J. Protocol for the Development of the
345 Master Chemical Mechanism, MCM v3 (Part A): Tropospheric Degradation of Non-Aromatic
346 Volatile Organic Compounds. *Atmos Chem Phys* **2003**, *3* (1), 161–180.
347 <https://doi.org/10.5194/acp-3-161-2003>.
- 348 (46) Jenkin, M. E.; Saunders, S. M.; Wagner, V.; Pilling, M. J. Protocol for the Development of the
349 Master Chemical Mechanism, MCM v3 (Part B): Tropospheric Degradation of Aromatic Volatile
350 Organic Compounds. *Part B* **2003**, *3* (1), 181–193. <https://doi.org/10.5194/acp-3-181-2003>.
- 351 (47) Buxton, G. V.; Greenstock, C. L.; Helman, W. P.; Ross, A. B. Critical Review of Rate Constants for
352 Reactions of Hydrated Electrons, Hydrogen Atoms and Hydroxyl Radicals ($\cdot\text{OH}/\cdot\text{O}^-$) in Aqueous
353 Solution. *J. Phys. Chem. Ref. Data* **1988**, *17* (2), 513–886. <https://doi.org/10.1063/1.555805>.
- 354 (48) Hoffman, M. Z.; Hayon, E. Pulse Radiolysis Study of Sulphydryl Compounds in Aqueous Solution.
355 *J. Phys. Chem.* **1973**, *77* (8), 990–996. <https://doi.org/10.1021/j100627a005>.
- 356 (49) Zhao, M. J.; Jung, L.; Tanielian, C.; Mechlin, R. Kinetics of the Competitive Degradation of
357 Deoxyribose and Other Biomolecules by Hydroxyl Radicals Produced by the Fenton Reaction.
358 *Free Radic. Res.* **1994**, *20* (6), 345–363. <https://doi.org/10.3109/10715769409145635>.
- 359 (50) Kanofsky, J. R.; Sima, P. D. Reactive Absorption of Ozone by Aqueous Biomolecule Solutions:
360 Implications for the Role of Sulphydryl Compounds as Targets for Ozone. *Arch. Biochem. Biophys.*
361 **1995**, *316* (1), 52–62. <https://doi.org/10.1006/abbi.1995.1009>.
- 362 (51) Pryor, W. A.; Giamalva, D. H.; Church, D. F. Kinetics of Ozonation. 2. Amino Acids and Model
363 Compounds in Water and Comparisons to Rates in Nonpolar Solvents. *J. Am. Chem. Soc.* **1984**,
364 *106* (23), 7094–7100. <https://doi.org/10.1021/ja00335a038>.

- 365 (52) Kim, H. I.; Kim, H.; Shin, Y. S.; Beegle, L. W.; Jang, S. S.; Neidholdt, E. L.; Goddard, W. A.; Heath, J.
366 R.; Kanik, I.; Beauchamp, J. L. Interfacial Reactions of Ozone with Surfactant Protein B in a Model
367 Lung Surfactant System. *J. Am. Chem. Soc.* **2010**, *132* (7), 2254–2263.
368 <https://doi.org/10.1021/ja908477w>.
- 369 (53) Hasson, A. S.; Ho, A. W.; Kuwata, K. T.; Paulson, S. E. Production of Stabilized Criegee
370 Intermediates and Peroxides in the Gas Phase Ozonolysis of Alkenes: 2. Asymmetric and
371 Biogenic Alkenes. *J. Geophys. Res. Atmospheres* **2001**, *106* (D24), 34143–34153.
372 <https://doi.org/10.1029/2001JD000598>.
- 373 (54) Hewitt, C. N.; Kok, G. L. Formation and Occurrence of Organic Hydroperoxides in the
374 Troposphere: Laboratory and Field Observations. *J. Atmospheric Chem.* **1991**, *12* (2), 181–194.
375 <https://doi.org/10.1007/BF00115779>.
- 376 (55) Zhou, Z.; Abbatt, J. P. D. Formation of Gas-Phase Hydrogen Peroxide via Multiphase Ozonolysis
377 of Unsaturated Lipids. *Environ. Sci. Technol. Lett.* **2021**, *8* (2), 114–120.
378 <https://doi.org/10.1021/acs.estlett.0c00757>.
- 379 (56) Navarrete, M.; Rangel, C.; Corchado, J. C.; Espinosa-García, J. Trapping of the OH Radical by α -
380 Tocopherol: A Theoretical Study. *J. Phys. Chem. A* **2005**, *109* (21), 4777–4784.
381 <https://doi.org/10.1021/jp050717e>.
- 382 (57) Kermani, S.; Ben-Jebria, A.; Ultman, J. S. Kinetics of Ozone Reaction with Uric Acid, Ascorbic
383 Acid, and Glutathione at Physiologically Relevant Conditions. *Arch. Biochem. Biophys.* **2006**, *451*
384 (1), 8–16. <https://doi.org/10.1016/j.abb.2006.04.015>.
- 385 (58) Rush, J. D.; Bielski, B. H. J. Pulse Radiolytic Studies of the Reaction of Perhydroxyl/Superoxide
386 O₂- with Iron(II)/Iron(III) Ions. The Reactivity of HO₂/O₂- with Ferric Ions and Its Implication on
387 the Occurrence of the Haber-Weiss Reaction. *J. Phys. Chem.* **1985**, *89* (23), 5062–5066.
388 <https://doi.org/10.1021/j100269a035>.
- 389 (59) Christensen, H.; Sehested, K.; Corfitzen, H. Reactions of Hydroxyl Radicals with Hydrogen
390 Peroxide at Ambient and Elevated Temperatures. *J. Phys. Chem.* **1982**, *86* (9), 1588–1590.
391 <https://doi.org/10.1021/j100206a023>.
- 392 (60) Sehested, K.; Rasmussen, O. L.; Fricke, H. Rate Constants of OH with HO₂, O₂-, and H₂O₂⁺ from
393 Hydrogen Peroxide Formation in Pulse-Irradiated Oxygenated Water. *J. Phys. Chem.* **1968**, *72*
394 (2), 626–631. <https://doi.org/10.1021/j100848a040>.
- 395 (61) Koppenol, W. H. The Haber-Weiss Cycle – 70 Years Later. *Redox Rep.* **2001**, *6* (4), 229–234.
396 <https://doi.org/10.1179/135100001101536373>.
- 397 (62) Jayson, G. G.; Parsons, B. J.; Swallow, A. J. Oxidation of Ferrous Ions by Perhydroxyl Radicals. *J.*
398 *Chem. Soc. Faraday Trans. 1 Phys. Chem. Condens. Phases* **1973**, *69*, 236–242.
399 <https://doi.org/10.1039/f19736900236>.
- 400 (63) Lewis, S.; Lynch, A.; Bachas, L.; Hampson, S.; Ormsbee, L.; Bhattacharyya, D. Chelate-Modified
401 Fenton Reaction for the Degradation of Trichloroethylene in Aqueous and Two-Phase Systems.
402 *Environ. Eng. Sci.* **2009**, *26* (4), 849–859. <https://doi.org/10.1089/ees.2008.0277>.
- 403 (64) Stuglik, Z.; PawełZagórski, Z. Pulse Radiolysis of Neutral Iron(II) Solutions: Oxidation of Ferrous
404 Ions by OH Radicals. *Radiat. Phys. Chem.* **1977** *1981*, *17* (4), 229–233.
405 [https://doi.org/10.1016/0146-5724\(81\)90336-8](https://doi.org/10.1016/0146-5724(81)90336-8).
- 406 (65) Masuda, T.; Shinohara, H.; Kondo, M. Reactions of Hydroxyl Radicals with Nucleic Acid Bases
407 and the Related Compounds in Gamma-Irradiated Aqueous Solution. *J. Radiat. Res. (Tokyo)*
408 **1978**, *16* (3), 153–161.
- 409 (66) Liphard, M.; Bothe, E.; Schulte-Frohlinde, D. The Influence of Glutathione on Single-Strand
410 Breakage in Single-Stranded DNA Irradiated in Aqueous Solution in the Absence and Presence of
411 Oxygen. *Int. J. Radiat. Biol.* **1990**, *58* (4), 589–602.
412 <https://doi.org/10.1080/09553009014551951>.

- 413 (67) Carr, A.; Lykkesfeldt, J. *Vitamin C in Health and Disease*; MDPI-Multidisciplinary Digital
414 Publishing Institute, 2018.
- 415 (68) Shen, J.; Griffiths, P. T.; Campbell, S. J.; Uttinger, B.; Kalberer, M.; Paulson, S. E. Ascorbate
416 Oxidation by Iron, Copper and Reactive Oxygen Species: Review, Model Development, and
417 Derivation of Key Rate Constants. *Sci. Rep.* **2021**, *11* (1), 7417. <https://doi.org/10.1038/s41598-021-86477-8>.
- 418 (69) Adams, G. E.; Boag, J. W.; Currant, J.; Michael, B. D. *Absolute Rate Constants for the Reaction of*
419 *the Hydroxyl Radical with Organic Compounds*; Pulse Radiolysis, 1965.
- 420 (70) Goldstein, S.; Lind, J.; Merenyi, G. Reaction of Organic Peroxyl Radicals with $\cdot\text{NO}_2$ and $\cdot\text{NO}$ in
421 Aqueous Solution: Intermediacy of Organic Peroxynitrate and Peroxynitrite Species. *J. Phys.*
422 *Chem. A* **2004**, *108* (10), 1719–1725. <https://doi.org/10.1021/jp037431z>.
- 423 (71) Jones, C. M.; Lawrence, A.; Wardman, P.; Burkitt, M. J. Electron Paramagnetic Resonance Spin
424 Trapping Investigation into the Kinetics of Glutathione Oxidation by the Superoxide Radical: Re-
425 Evaluation of the Rate Constant. *Free Radic. Biol. Med.* **2002**, *32* (10), 982–990.
426 [https://doi.org/10.1016/S0891-5849\(02\)00791-8](https://doi.org/10.1016/S0891-5849(02)00791-8).
- 427 (72) Winterbourn, C. C.; Metodiewa, D. The Reaction of Superoxide with Reduced Glutathione. *Arch.*
428 *Biochem. Biophys.* **1994**, *314* (2), 284–290. <https://doi.org/10.1006/abbi.1994.1444>.
- 429 (73) Wefers, H.; Sies, H. Oxidation of Glutathione by the Superoxide Radical to the Disulfide and the
430 Sulfonate Yielding Singlet Oxygen. *Eur. J. Biochem.* **1983**, *137* (1–2), 29–36.
431 <https://doi.org/10.1111/j.1432-1033.1983.tb07791.x>.
- 432 (74) Ford, E.; Hughes, M. N.; Wardman, P. Kinetics of the Reactions of Nitrogen Dioxide with
433 Glutathione, Cysteine, and Uric Acid at Physiological PH. *Free Radic. Biol. Med.* **2002**, *32* (12),
434 1314–1323. [https://doi.org/10.1016/S0891-5849\(02\)00850-X](https://doi.org/10.1016/S0891-5849(02)00850-X).
- 435 (75) Luo, D.; Smith, S. W.; Anderson, B. D. Kinetics and Mechanism of the Reaction of Cysteine and
436 Hydrogen Peroxide in Aqueous Solution. *J. Pharm. Sci.* **2005**, *94* (2), 304–316.
437 <https://doi.org/10.1002/jps.20253>.
- 438 (76) Winkler, B. S.; Orselli, S. M.; Rex, T. S. The Redox Couple between Glutathione and Ascorbic
439 Acid: A Chemical and Physiological Perspective. *Free Radic. Biol. Med.* **1994**, *17* (4), 333–349.
440 [https://doi.org/10.1016/0891-5849\(94\)90019-1](https://doi.org/10.1016/0891-5849(94)90019-1).
- 441 (77) Buettner, G. R.; Jurkiewicz, B. A. Catalytic Metals, Ascorbate and Free Radicals: Combinations to
442 Avoid. *Radiat. Res.* **1996**, *145* (5), 532. <https://doi.org/10.2307/3579271>.
- 443 (78) Alfassi, Z. B.; Huie, R. E.; Neta, P.; Shoute, L. C. T. Temperature Dependence of the Rate
444 Constants for Reaction of Inorganic Radicals with Organic Reductants. *J. Phys. Chem.* **1990**, *94*
445 (25), 8800–8805. <https://doi.org/10.1021/j100388a011>.
- 446 (79) Augusto, O.; Bonini, M. G.; Amanso, A. M.; Linares, E.; Santos, C. C. X.; De Menezes, S. L.
447 Nitrogen Dioxide and Carbonate Radical Anion: Two Emerging Radicals in Biology. *Free Radic.*
448 *Biol. Med.* **2002**, *32* (9), 841–859. [https://doi.org/10.1016/S0891-5849\(02\)00786-4](https://doi.org/10.1016/S0891-5849(02)00786-4).
- 449 (80) Goldstein, S.; Czapski, G. Reactivity of Peroxynitrite versus Simultaneous Generation of $\cdot\text{NO}$ and
450 $\text{O}_2^{\cdot-}$ toward NADH. *Chem. Res. Toxicol.* **2000**, *13* (8), 736–741.
451 <https://doi.org/10.1021/tx000099n>.
- 452 (81) Graetzel, M. Pulsradiolytische Untersuchung einiger Elementarprozesse der Oxydation und
453 Reduktion des Nitritions. *Berichte Bunsenges. Fuer Phys. Chem.* **1969**, *73* (7).
- 454 (82) Jacob, D. Heterogeneous Chemistry and Tropospheric Ozone. *Atmos. Environ.* **2000**, *34* (12–14),
455 2131–2159. [https://doi.org/10.1016/S1352-2310\(99\)00462-8](https://doi.org/10.1016/S1352-2310(99)00462-8).
- 456 (83) Bonini, M. G.; Augusto, O. Carbon Dioxide Stimulates the Production of Thiyl, Sulfinyl, and
457 Disulfide Radical Anion from Thiol Oxidation by Peroxynitrite. *J. Biol. Chem.* **2001**, *276* (13),
458 9749–9754. <https://doi.org/10.1074/jbc.M008456200>.

- 460 (84) Kurz, C. R.; Kissner, R.; Nauser, T.; Perrin, D.; Koppenol, W. H. Rapid Scavenging of Peroxynitrous
461 Acid by Monohydroascorbate. *Free Radic. Biol. Med.* **2003**, *35* (12), 1529–1537.
462 <https://doi.org/10.1016/j.freeradbiomed.2003.08.012>.
- 463 (85) Squadrito, G. L.; Cueto, R.; Splenser, A. E.; Valavanidis, A.; Zhang, H.; Uppu, R. M.; Pryor, W. A.
464 Reaction of Uric Acid with Peroxynitrite and Implications for the Mechanism of Neuroprotection
465 by Uric Acid. *Arch. Biochem. Biophys.* **2000**, *376* (2), 333–337.
466 <https://doi.org/10.1006/abbi.2000.1721>.
- 467 (86) Arana, A. A.; Artaxo, P.; Rizzo, L. V.; Bastos, W. Long Term Measurements of the Elemental
468 Composition and Optical Properties of Aerosols in Amazonia. *E3S Web Conf.* **2013**, *1*, 03005.
469 <https://doi.org/10.1051/e3sconf/20130103005>.
- 470 (87) Birmili, W.; Allen, A. G.; Bary, F.; Harrison, R. M. Trace Metal Concentrations and Water
471 Solubility in Size-Fractionated Atmospheric Particles and Influence of Road Traffic. *Environ. Sci.
472 Technol.* **2006**, *40* (4), 1144–1153. <https://doi.org/10.1021/es0486925>.
- 473 (88) Heal, M. R.; Hibbs, L. R.; Agius, R. M.; Beverland, I. J. Total and Water-Soluble Trace Metal
474 Content of Urban Background PM₁₀, PM_{2.5} and Black Smoke in Edinburgh, UK. *Atmos. Environ.*
475 **2005**, *39* (8), 1417–1430. <https://doi.org/10.1016/j.atmosenv.2004.11.026>.
- 476 (89) Harrison, R. M.; Yin, J. Chemical Speciation of PM_{2.5} Particles at Urban Background and Rural
477 Sites in the UK Atmosphere. *J. Environ. Monit.* **2010**, *12* (7), 1404–1414.
478 <https://doi.org/10.1039/c000329h>.
- 479 (90) Maenhaut, W.; Salma, I.; Cafmeyer, J.; Annegarn, H. J.; Andreae, M. O. Regional Atmospheric
480 Aerosol Composition and Sources in the Eastern Transvaal, South Africa, and Impact of Biomass
481 Burning. *J. Geophys. Res. Atmospheres* **1996**, *101* (D19), 23631–23650.
482 <https://doi.org/10.1029/95JD02930>.
- 483 (91) Artaxo, P.; Gerab, F.; Yamasoe, M. A.; Martins, J. V. Fine Mode Aerosol Composition at Three
484 Long-Term Atmospheric Monitoring Sites in the Amazon Basin. *J. Geophys. Res.* **1994**, *99* (D11),
485 22857–22868. <https://doi.org/10.1029/94JD01023>.
- 486 (92) Pakkanen, T. A.; Loukkola, K.; Korhonen, C. H.; Aurela, M.; Mäkelä, T.; Hillamo, R. E.; Aarnio, P.;
487 Koskentalo, T.; Kousa, A.; Maenhaut, W. Sources and Chemical Composition of Atmospheric Fine
488 and Coarse Particles in the Helsinki Area. *Atmos. Environ.* **2001**, *35* (32), 5381–5391.
489 [https://doi.org/10.1016/S1352-2310\(01\)00307-7](https://doi.org/10.1016/S1352-2310(01)00307-7).
- 490 (93) Olson, D. A.; Turlington, J.; Duvall, R. M.; McDow, S. R.; Stevens, C. D.; Williams, R. Indoor and
491 Outdoor Concentrations of Organic and Inorganic Molecular Markers: Source Apportionment of
492 PM_{2.5} Using Low-Volume Samples. *Atmos. Environ.* **2008**, *42* (8), 1742–1751.
493 <https://doi.org/10.1016/j.atmosenv.2007.11.035>.
- 494 (94) Lee, P. K. H.; Brook, J. R.; Dabek-Zlotorzynska, E.; Mabury, S. A. Identification of the Major
495 Sources Contributing to PM_{2.5} Observed in Toronto. *Environ. Sci. Technol.* **2003**, *37* (21), 4831–
496 4840. <https://doi.org/10.1021/es026473i>.
- 497 (95) Upadhyay, N.; Clements, A.; Fraser, M.; Herckes, P. Chemical Speciation of PM_{2.5} and PM₁₀ in
498 South Phoenix, AZ. *J. Air Waste Manag. Assoc.* **2011**, *61* (3), 302–310.
499 <https://doi.org/10.3155/1047-3289.61.3.302>.
- 500 (96) Hassanvand, M. S.; Naddafi, K.; Faridi, S.; Nabizadeh, R.; Sowlat, M. H.; Momeniha, F.;
501 Gholampour, A.; Arhami, M.; Kashani, H.; Zare, A.; Niazi, S.; Rastkari, N.; Nazmara, S.; Ghani, M.;
502 Yunesian, M. Characterization of PAHs and Metals in Indoor/Outdoor PM10/PM2.5/PM1 in a
503 Retirement Home and a School Dormitory. *Sci. Total Environ.* **2015**, *527–528*, 100–110.
504 <https://doi.org/10.1016/j.scitotenv.2015.05.001>.
- 505 (97) Contini, D.; Cesari, D.; Donateo, A.; Chirizzi, D.; Belosi, F. Characterization of PM10 and PM2.5
506 and Their Metals Content in Different Typologies of Sites in South-Eastern Italy. *Atmosphere*
507 **2014**, *5* (2), 435–453. <https://doi.org/10.3390/atmos5020435>.

- 508 (98) Manousakas, M.; Papaefthymiou, H.; Eleftheriadis, K.; Katsanou, K. Determination of Water-
509 Soluble and Insoluble Elements in PM2.5 by ICP-MS. *Sci. Total Environ.* **2014**, *493*, 694–700.
510 <https://doi.org/10.1016/j.scitotenv.2014.06.043>.
- 511 (99) Han, Y.-J.; Kim, H.-W.; Cho, S.-H.; Kim, P.-R.; Kim, W.-J. Metallic Elements in PM2.5 in Different
512 Functional Areas of Korea: Concentrations and Source Identification. *Atmospheric Res.* **2015**,
513 *153*, 416–428. <https://doi.org/10.1016/j.atmosres.2014.10.002>.
- 514 (100) Maenhaut, W.; Raes, N.; Chi, X.; Cafmeyer, J.; Wang, W.; Salma, I. Chemical Composition and
515 Mass Closure for Fine and Coarse Aerosols at a Kerbside in Budapest, Hungary, in Spring 2002.
516 *X-Ray Spectrom.* **2005**, *34* (4), 290–296. <https://doi.org/10.1002/xrs.820>.
- 517 (101) Rogula-Kozłowska, W.; Błaszcak, B.; Szopa, S.; Klejnowski, K.; Sówka, I.; Zwoździak, A.;
518 Jabłońska, M.; Mathews, B. PM2.5 in the Central Part of Upper Silesia, Poland: Concentrations,
519 Elemental Composition, and Mobility of Components. *Environ. Monit. Assess.* **2013**, *185* (1),
520 581–601. <https://doi.org/10.1007/s10661-012-2577-1>.
- 521 (102) Morishita, M.; Keeler, G. J.; Kamal, A. S.; Wagner, J. G.; Harkema, J. R.; Rohr, A. C. Identification
522 of Ambient PM2.5 Sources and Analysis of Pollution Episodes in Detroit, Michigan Using Highly
523 Time-Resolved Measurements. *Atmos. Environ.* **2011**, *45* (8), 1627–1637.
524 <https://doi.org/10.1016/j.atmosenv.2010.09.062>.
- 525 (103) Chow, J. C.; Watson, J. G.; Fujita, E. M.; Lu, Z.; Lawson, D. R.; Ashbaugh, L. L. Temporal and
526 Spatial Variations of PM2.5 and PM10 Aerosol in the Southern California Air Quality Study.
527 *Atmos. Environ.* **1994**, *28* (12), 2061–2080. [https://doi.org/10.1016/1352-2310\(94\)90474-X](https://doi.org/10.1016/1352-2310(94)90474-X).
- 528 (104) Vecchi, R.; Marcazzan, G.; Valli, G.; Ceriani, M.; Antoniazzi, C. The Role of Atmospheric
529 Dispersion in the Seasonal Variation of PM1 and PM2.5 Concentration and Composition in the
530 Urban Area of Milan (Italy). *Atmos. Environ.* **2004**, *38* (27), 4437–4446.
531 <https://doi.org/10.1016/j.atmosenv.2004.05.029>.
- 532 (105) Khodeir, M.; Shamy, M.; Alghamdi, M.; Zhong, M.; Sun, H.; Costa, M.; Chen, L.-C.; Maciejczyk, P.
533 Source Apportionment and Elemental Composition of PM2.5 and PM10 in Jeddah City, Saudi
534 Arabia. *Atmospheric Pollut. Res.* **2012**, *3* (3), 331–340. <https://doi.org/10.5094/APR.2012.037>.
- 535 (106) Hagler, G. S. W.; Bergin, M. H.; Salmon, L. G.; Yu, J. Z.; Wan, E. C. H.; Zheng, M.; Zeng, L. M.;
536 Kiang, C. S.; Zhang, Y. H.; Schauer, J. J. Local and Regional Anthropogenic Influence on PM2.5
537 Elements in Hong Kong. *Atmos. Environ.* **2007**, *41* (28), 5994–6004.
538 <https://doi.org/10.1016/j.atmosenv.2007.03.012>.
- 539 (107) Loyola, J.; Arbillia, G.; Quiterio, S. L.; Escaleira, V.; Minho, A. S. Trace Metals in the Urban
540 Aerosols of Rio de Janeiro City. *J. Braz. Chem. Soc.* **2012**, *23* (4), 628–638.
541 <https://doi.org/10.1590/S0103-50532012000400007>.
- 542 (108) Squizzato, S.; Masiol, M.; Visin, F.; Canal, A.; Rampazzo, G.; Pavoni, B. The PM2.5 Chemical
543 Composition in an Industrial Zone Included in a Large Urban Settlement: Main Sources and Local
544 Background. *Environ. Sci. Process. Impacts* **2014**, *16* (8), 1913–1922.
545 <https://doi.org/10.1039/C4EM00111G>.
- 546 (109) Matschullat, J.; Maenhaut, W.; Zimmermann, F.; Juliane Fiebig. Aerosol and Bulk Deposition
547 Trends in the 1990's, Eastern Erzgebirge, Central Europe. *Atmos. Environ.* **2000**, *34* (19), 3213–
548 3221. [https://doi.org/10.1016/S1352-2310\(99\)00516-6](https://doi.org/10.1016/S1352-2310(99)00516-6).
- 549 (110) Querol, X.; Alastuey, A.; Rodriguez, S.; Plana, F.; Ruiz, C. R.; Cots, N.; Massagué, G.; Puig, O.
550 PM10 and PM2.5 Source Apportionment in the Barcelona Metropolitan Area, Catalonia, Spain.
551 *Atmos. Environ.* **2001**, *35* (36), 6407–6419. [https://doi.org/10.1016/S1352-2310\(01\)00361-2](https://doi.org/10.1016/S1352-2310(01)00361-2).
- 552 (111) Martinez, M. A.; Caballero, P.; Carrillo, O.; Mendoza, A.; Mejia, G. M. Chemical Characterization
553 and Factor Analysis of PM_{2.5} in Two Sites of Monterrey, Mexico. *J. Air Waste Manag. Assoc.*
554 **2012**, *62* (7), 817–827. <https://doi.org/10.1080/10962247.2012.681421>.

- 555 (112) Janssen, N. A. H.; Van Mansom, D. F. M.; Van Der Jagt, K.; Harssema, H.; Hoek, G. Mass
556 Concentration and Elemental Composition of Airborne Particulate Matter at Street and
557 Background Locations. *Atmos. Environ.* **1997**, *31* (8), 1185–1193.
558 [https://doi.org/10.1016/S1352-2310\(96\)00291-9](https://doi.org/10.1016/S1352-2310(96)00291-9).
- 559 (113) Na, K.; Cocker, D. R. Characterization and Source Identification of Trace Elements in PM_{2.5} from
560 Mira Loma, Southern California. *Atmospheric Res.* **2009**, *93* (4), 793–800.
561 <https://doi.org/10.1016/j.atmosres.2009.03.012>.
- 562 (114) Shaltout, A. A.; Boman, J.; Al-Malawi, D. R.; Shehadeh, Z. F. Elemental Composition of PM_{2.5}
563 Particles Sampled in Industrial and Residential Areas of Taif, Saudi Arabia. *Aerosol Air Qual. Res.*
564 **2013**, *13* (4), 1356–1364. <https://doi.org/10.4209/aaqr.2012.11.0320>.
- 565 (115) Chow, J. C.; Watson, J. G.; Lu, Z.; Lowenthal, D. H.; Frazier, C. A.; Solomon, P. A.; Thuillier, R. H.;
566 Magliano, K. Descriptive Analysis of PM_{2.5} and PM₁₀ at Regionally Representative Locations
567 during SJVAQS/AUSPEX. *Atmos. Environ.* **1996**, *30* (12), 2079–2112.
568 [https://doi.org/10.1016/1352-2310\(95\)00402-5](https://doi.org/10.1016/1352-2310(95)00402-5).
- 569 (116) Kendall, M.; Pala, K.; Ucakli, S.; Gucer, S. Airborne Particulate Matter (PM_{2.5} and PM₁₀) and
570 Associated Metals in Urban Turkey. *Air Qual. Atmosphere Health* **2011**, *4* (3–4), 235–242.
571 <https://doi.org/10.1007/s11869-010-0129-9>.
- 572 (117) Mansha, M.; Ghauri, B.; Rahman, S.; Amman, A. Characterization and Source Apportionment of
573 Ambient Air Particulate Matter (PM_{2.5}) in Karachi. *Sci. Total Environ.* **2012**, *425*, 176–183.
574 <https://doi.org/10.1016/j.scitotenv.2011.10.056>.
- 575 (118) Pant, P.; Shukla, A.; Kohl, S. D.; Chow, J. C.; Watson, J. G.; Harrison, R. M. Characterization of
576 Ambient PM_{2.5} at a Pollution Hotspot in New Delhi, India and Inference of Sources. *Atmos.*
577 *Environ.* **2015**, *109*, 178–189. <https://doi.org/10.1016/j.atmosenv.2015.02.074>.
- 578 (119) Tolis, E. I.; Saraga, D. E.; Filiou, K. F.; Tziavos, N. I.; Tsiaousis, C. P.; Dinas, A.; Bartzis, J. G. One-
579 Year Intensive Characterization on PM_{2.5} Nearby Port Area of Thessaloniki, Greece. *Environ. Sci.*
580 *Pollut. Res.* **2015**, *22* (9), 6812–6826. <https://doi.org/10.1007/s11356-014-3883-7>.
- 581 (120) López, M. L.; Ceppi, S.; Palancar, G. G.; Olcese, L. E.; Tirao, G.; Toselli, B. M. Elemental
582 Concentration and Source Identification of PM₁₀ and PM_{2.5} by SR-XRF in Córdoba City,
583 Argentina. *Atmos. Environ.* **2011**, *45* (31), 5450–5457.
584 <https://doi.org/10.1016/j.atmosenv.2011.07.003>.
- 585 (121) Cao, L.; Zeng, J.; Liu, K.; Bao, L.; Li, Y. Characterization and Cytotoxicity of PM<0.2, PM_{0.2–2.5}
586 and PM_{2.5–10} around MSWI in Shanghai, China. *Int. J. Environ. Res. Public. Health* **2015**, *12* (5),
587 5076–5089. <https://doi.org/10.3390/ijerph120505076>.
- 588 (122) Yin, L.; Niu, Z.; Chen, X.; Chen, J.; Xu, L.; Zhang, F. Chemical Compositions of PM_{2.5} Aerosol
589 during Haze Periods in the Mountainous City of Yong'an, China. *J. Environ. Sci.* **2012**, *24* (7),
590 1225–1233. [https://doi.org/10.1016/S1001-0742\(11\)60940-6](https://doi.org/10.1016/S1001-0742(11)60940-6).
- 591 (123) Zhou, S.; Yuan, Q.; Li, W.; Lu, Y.; Zhang, Y.; Wang, W. Trace Metals in Atmospheric Fine Particles
592 in One Industrial Urban City: Spatial Variations, Sources, and Health Implications. *J. Environ. Sci.*
593 **2014**, *26* (1), 205–213. [https://doi.org/10.1016/S1001-0742\(13\)60399-X](https://doi.org/10.1016/S1001-0742(13)60399-X).
- 594 (124) Wang, X.; Bi, X.; Sheng, G.; Fu, J. Chemical Composition and Sources of PM₁₀ and PM_{2.5}
595 Aerosols in Guangzhou, China. *Environ. Monit. Assess.* **2006**, *119* (1–3), 425–439.
596 <https://doi.org/10.1007/s10661-005-9034-3>.
- 597 (125) Kulshrestha, A.; Satsangi, P. G.; Masih, J.; Taneja, A. Metal Concentration of PM_{2.5} and PM₁₀
598 Particles and Seasonal Variations in Urban and Rural Environment of Agra, India. *Sci. Total*
599 *Environ.* **2009**, *407* (24), 6196–6204. <https://doi.org/10.1016/j.scitotenv.2009.08.050>.
- 600 (126) Yadav, S.; Satsangi, P. G. Characterization of Particulate Matter and Its Related Metal Toxicity in
601 an Urban Location in South West India. *Environ. Monit. Assess.* **2013**, *185* (9), 7365–7379.
602 <https://doi.org/10.1007/s10661-013-3106-6>.

- 603 (127) Song, S.; Wu, Y.; Jiang, J.; Yang, L.; Cheng, Y.; Hao, J. Chemical Characteristics of Size-Resolved
604 PM_{2.5} at a Roadside Environment in Beijing, China. *Environ. Pollut.* **2012**, *161*, 215–221.
605 <https://doi.org/10.1016/j.envpol.2011.10.014>.
- 606 (128) Sun, Y.; Zhuang, G.; Wang, Y.; Han, L.; Guo, J.; Dan, M.; Zhang, W.; Wang, Z.; Hao, Z. The Air-
607 Borne Particulate Pollution in Beijing—Concentration, Composition, Distribution and Sources.
608 *Atmos. Environ.* **2004**, *38* (35), 5991–6004. <https://doi.org/10.1016/j.atmosenv.2004.07.009>.
- 609 (129) See, S. W.; Balasubramanian, R.; Rianawati, E.; Karthikeyan, S.; Streets, D. G. Characterization
610 and Source Apportionment of Particulate Matter ≤ 2.5 Mm in Sumatra, Indonesia, during a
611 Recent Peat Fire Episode. *Environ. Sci. Technol.* **2007**, *41* (10), 3488–3494.
612 <https://doi.org/10.1021/es061943k>.
- 613 (130) Poschl, U.; Martin, S. T.; Sinha, B.; Chen, Q.; Gunthe, S. S.; Huffman, J. A.; Borrmann, S.; Farmer,
614 D. K.; Garland, R. M.; Helas, G.; Jimenez, J. L.; King, S. M.; Manzi, A.; Mikhailov, E.; Pauliquevis,
615 T.; Petters, M. D.; Prenni, A. J.; Roldin, P.; Rose, D.; Schneider, J.; Su, H.; Zorn, S. R.; Artaxo, P.;
616 Andreae, M. O. Rainforest Aerosols as Biogenic Nuclei of Clouds and Precipitation in the
617 Amazon. *Science* **2010**, *329* (5998), 1513–1516. <https://doi.org/10.1126/science.1191056>.
- 618 (131) Jimenez, J. L.; Canagaratna, M. R.; Donahue, N. M.; Prevot, A. S. H.; Zhang, Q.; Kroll, J. H.;
619 DeCarlo, P. F.; Allan, J. D.; Coe, H.; Ng, N. L.; Aiken, A. C.; Docherty, K. S.; Ulbrich, I. M.; Grieshop,
620 A. P.; Robinson, A. L.; Duplissy, J.; Smith, J. D.; Wilson, K. R.; Lanz, V. A.; Hueglin, C.; Sun, Y. L.;
621 Tian, J.; Laaksonen, A.; Raatikainen, T.; Rautiainen, J.; Vaattovaara, P.; Ehn, M.; Kulmala, M.;
622 Tomlinson, J. M.; Collins, D. R.; Cubison, M. J.; E.; Dunlea, J.; Huffman, J. A.; Onasch, T. B.;
623 Alfarra, M. R.; Williams, P. I.; Bower, K.; Kondo, Y.; Schneider, J.; Drewnick, F.; Borrmann, S.;
624 Weimer, S.; Demerjian, K.; Salcedo, D.; Cottrell, L.; Griffin, R.; Takami, A.; Miyoshi, T.;
625 Hatakeyama, S.; Shimono, A.; Sun, J. Y.; Zhang, Y. M.; Dzepina, K.; Kimmel, J. R.; Sueper, D.;
626 Jayne, J. T.; Herndon, S. C.; Trimborn, A. M.; Williams, L. R.; Wood, E. C.; Middlebrook, A. M.;
627 Kolb, C. E.; Baltensperger, U.; Worsnop, D. R. Evolution of Organic Aerosols in the Atmosphere.
628 *Science* **2009**, *326* (5959), 1525–1529. <https://doi.org/10.1126/science.1180353>.
- 629 (132) Huang, R.-J.; Zhang, Y.; Bozzetti, C.; Ho, K.-F.; Cao, J.-J.; Han, Y.; Daellenbach, K. R.; Slowik, J. G.;
630 Platt, S. M.; Canonaco, F.; Zotter, P.; Wolf, R.; Pieber, S. M.; Bruns, E. A.; Crippa, M.; Ciarelli, G.;
631 Piazzalunga, A.; Schwikowski, M.; Abbaszade, G.; Schnelle-Kreis, J.; Zimmermann, R.; An, Z.;
632 Szidat, S.; Baltensperger, U.; Haddad, I. E.; Prévôt, A. S. H. High Secondary Aerosol Contribution
633 to Particulate Pollution during Haze Events in China. *Nature* **2014**, *514* (7521), 218–222.
634 <https://doi.org/10.1038/nature13774>.
- 635 (133) Wingfors, H. Characterization of the Size-Distribution of Aerosols and Particle-Bound Content of
636 Oxygenated PAHs, PAHs, and n-Alkanes in Urban Environments in Afghanistan. *Atmos. Environ.*
637 **2011**, *45* (26), 4360–4369. <https://doi.org/10.1016/j.atmosenv.2011.05.049>.
- 638 (134) Valavanidis, A.; Fiotakis, K.; Vlahogianni, T.; Papadimitriou, V.; Pantikaki, V. Determination of
639 Selective Quinones and Quinoid Radicals in Airborne Particulate Matter and Vehicular Exhaust
640 Particles. *Environ. Chem.* **2006**, *3* (2), 118–123. <https://doi.org/10.1071/EN05089>.
- 641 (135) Eiguren-Fernandez, A.; Miguel, A. H.; Di Stefano, E.; Schmitz, D. A.; Cho, A. K.; Thurairatnam, S.;
642 Avol, E. L.; Froines, J. R. Atmospheric Distribution of Gas- and Particle-Phase Quinones in
643 Southern California. *Aerosol Sci. Technol.* **2008**, *42* (10), 854–861.
644 <https://doi.org/10.1080/02786820802339546>.
- 645 (136) Delgado-Saborit, J. M.; Alam, M. S.; Godri Pollitt, K. J.; Stark, C.; Harrison, R. M. Analysis of
646 Atmospheric Concentrations of Quinones and Polycyclic Aromatic Hydrocarbons in Vapour and
647 Particulate Phases. *Atmos. Environ.* **2013**, *77*, 974–982.
648 <https://doi.org/10.1016/j.atmosenv.2013.05.080>.

- 649 (137) Alam, M. S.; Delgado-Saborit, J. M.; Stark, C.; Harrison, R. M. Investigating PAH Relative
650 Reactivity Using Congener Profiles, Quinone Measurements and Back Trajectories. *Atmospheric*
651 *Chem. Phys.* **2014**, *14* (5), 2467–2477. <https://doi.org/10.5194/acp-14-2467-2014>.
- 652 (138) Cho, A. K.; Di Stefano, E.; You, Y.; Rodriguez, C. E.; Schmitz, D. A.; Kumagai, Y.; Miguel, A. H.;
653 Eiguren-Fernandez, A.; Kobayashi, T.; Avol, E.; Froines, J. R. Determination of Four Quinones in
654 Diesel Exhaust Particles, SRM 1649a, and Atmospheric PM_{2.5} Special Issue of *Aerosol Science*
655 and Technology on Findings from the Fine Particulate Matter Supersites Program. *Aerosol Sci.*
656 *Technol.* **2004**, *38* (sup1), 68–81. <https://doi.org/10.1080/02786820390229471>.
- 657

Table S1. Chemical reactions, rate constants as used in the KM-SUB-ELF, with reference

#	Reaction	Rate constant (cm ⁻³ s ⁻¹ or s ⁻¹)	Reference
<i>Gas-phase reactions</i>			
1	NO [•] + O ₃ → NO ₂ [•] + O ₂	2.05 × 10 ⁻¹⁴	45,46
2	NO ₂ [•] + O ₃ → NO ₃ [•] + O ₂	4.85 × 10 ⁻¹⁷	45,46
3	NO [•] + NO [•] + O ₂ → NO ₂ [•] + NO ₂ [•]	8.93 × 10 ⁻²⁰	45,46
4	NO [•] + NO ₃ [•] → NO ₂ [•] + NO ₂ [•]	2.57 × 10 ⁻¹¹	45,46
5	NO ₂ [•] + NO ₃ [•] → NO [•] + NO ₂ [•] + O ₂	7.73 × 10 ⁻¹⁶	45,46
6	NO ₂ [•] + NO ₃ [•] → N ₂ O ₅	1.21 × 10 ⁻¹²	45,46
7	•OH + O ₃ → HO ₂ [•] + O ₂	8.20 × 10 ⁻¹⁴	45,46
8	•OH + H ₂ O ₂ → HO ₂ [•] + H ₂ O	1.73 × 10 ⁻¹²	45,46
9	HO ₂ [•] + O ₃ → •OH + O ₂ + O ₂	8.24 × 10 ⁻¹⁶	45,46
10	•OH + HO ₂ [•] → H ₂ O + O ₂	1.08 × 10 ⁻¹⁰	45,46
11	HO ₂ [•] + HO ₂ [•] → H ₂ O ₂ + O ₂	5.09 × 10 ⁻¹²	45,46
12	HO ₂ [•] + HO ₂ [•] → H ₂ O ₂	3.50 × 10 ⁻¹²	45,46
13	•OH + NO [•] → HONO	8.91 × 10 ⁻¹²	45,46
14	•OH + NO ₂ [•] → HNO ₃	8.91 × 10 ⁻¹²	45,46
15	•OH + NO ₃ [•] → HO ₂ [•] + NO ₂ [•]	2.00 × 10 ⁻¹¹	45,46
16	HO ₂ [•] + NO [•] → •OH + NO ₂ [•]	8.24 × 10 ⁻¹²	45,46
17	HO ₂ [•] + NO ₂ [•] → HO ₂ NO ₂	6.87 × 10 ⁻¹³	45,46
18	HO ₂ NO ₂ → HO ₂ [•] + NO ₂ [•]	2.49 × 10 ⁻¹	45,46
19	•OH + HO ₂ NO ₂ → NO ₂ [•] + H ₂ O + O ₂	2.96 × 10 ⁻¹²	45,46
20	HO ₂ [•] + NO ₃ [•] → •OH + NO ₂ [•]	4.00 × 10 ⁻¹²	45,46
21	•OH + HONO → NO ₂ [•] + H ₂ O	5.78 × 10 ⁻¹²	45,46
22	•OH + HNO ₃ → NO ₃ [•] + H ₂ O	1.37 × 10 ⁻¹³	45,46
23	N ₂ O ₅ → NO ₂ [•] + NO ₃ [•]	1.83 × 10 ⁻¹	45,46
<i>Surfactant reactions</i>			
24	SPB + •OH → SPB-ox	1.70 × 10 ⁻¹¹	47–49
25	POG + •OH → POG-ox	1.70 × 10 ⁻¹¹	1
26	SPB + O ₃ → SPB-ox	1.00 × 10 ⁻¹⁴	50,51
27	POG + O ₃ → POG-ox + 0.17 H ₂ O ₂	1.66 × 10 ⁻¹⁶	52–55
28	aToc + OH → aToc-ox	4.50 × 10 ⁻¹³	56
29	aToc + O ₃ → aToc-ox	1.20 × 10 ⁻¹⁸	57
<i>ELF reactions</i>			
30	O ₂ ^{•-} + HO ₂ + H ₂ O → H ₂ O ₂ + OH [•] + O ₂	1.70 × 10 ⁻¹³	1,58
31	HO ₂ + HO ₂ → H ₂ O ₂ + O ₂	1.40 × 10 ⁻¹⁵	58

32	$O_2^{\bullet\bullet} + O_2^{\bullet\bullet} + 2H^+ \rightarrow H_2O_2 + O_2$	3.82×10^{-16}	58
33	$H_2O_2 + \cdot OH \rightarrow HO_2 + H_2O$	5.50×10^{-14}	59
34	$\cdot OH + \cdot OH \rightarrow H_2O_2$	8.60×10^{-12}	60
35	$\cdot OH + O_2^{\bullet\bullet} \rightarrow O_2 + OH^-$	1.30×10^{-11}	47
36	$\cdot OH + HO_2 \rightarrow H_2O + O_2$	1.20×10^{-11}	60
37	$H_2O_2 + HO_2 \rightarrow \cdot OH + O_2 + H_2O$	4.98×10^{-21}	61
38	$Fe^{2+} + O_2^- + 2H^+ \rightarrow Fe^{3+} + H_2O_2$	3.10×10^{-14}	1,58
39	$Fe^{2+} + HO_2 + H^+ \rightarrow Fe^{3+} + H_2O_2$	1.99×10^{-15}	62
40	$Fe^{2+} + H_2O_2 \rightarrow Fe^{3+} + \cdot OH + OH^-$	4.30×10^{-18}	63
41	$Fe^{2+} + \cdot OH \rightarrow Fe^{3+} + OH^-$	5.30×10^{-13}	64
42	$Fe^{2+} + H_2O_2 \rightarrow Fe^{4+} + H_2O$	9.50×10^{-18}	1
43	$Fe^{3+} + H_2O_2 \rightarrow Fe^{2+} + HO_2 + H^+$	3.32×10^{-24}	63
44	$Fe^{3+} + HO_2 \rightarrow Fe^{2+} + O_2 + H^+$	3.30×10^{-18}	58
45	$Fe^{4+} + Fe^{2+} \rightarrow Fe^{3+} + Fe^{3+}$	6.60×10^{-18}	41
46	$Fe^{3+} + AscH \rightarrow Fe^{2+} + Asc^\bullet$	1.10×10^{-19}	1
47	$Fe^{4+} + AscH \rightarrow Fe^{3+} + Asc^\bullet$	7.60×10^{-19}	1
48	$Fe^{2+} + O_2 \rightarrow O_2^{\bullet\bullet} + Fe^{3+}$	5.20×10^{-21}	1
49	$Cu^+ + HO_2 + H^+ \rightarrow Cu^{2+} + H_2O_2$	2.30×10^{-12}	1
50	$Cu^+ + O_2^{\bullet\bullet} + H_2O \rightarrow Cu^{2+} + H_2O_2 + OH^-$	5.80×10^{-15}	1
51	$Cu^{2+} + HO_2 \rightarrow Cu^+ + O_2 + H^+$	1.60×10^{-11}	1
52	$Cu^{2+} + O_2^{\bullet\bullet} \rightarrow Cu^+ + O_2$	8.30×10^{-12}	1
53	$Cu^{2+} + AscH \rightarrow Cu^+ + Asc^\bullet$	1.40×10^{-18}	1
54	$Cu^+ + O_2 \rightarrow Cu^{2+} + O_2^{\bullet\bullet}$	6.90×10^{-20}	1
55	$Cu^+ + H_2O_2 \rightarrow Cu^{2+} + \cdot OH + OH^-$	2.40×10^{-20}	1
56	$Cu^+ + H_2O_2 \rightarrow Cu^{3+} + OH^- + OH^-$	5.00×10^{-19}	1
57	$Cu^+ + Cu^{3+} \rightarrow Cu^{2+} + Cu^{2+}$	5.80×10^{-12}	1
58	$Cu^{2+} + H_2O_2 \rightarrow Cu^+ + O_2^{\bullet\bullet} + H^+$	3.80×10^{-24}	1
59	$PQN + AscH \rightarrow PQN^\bullet + Asc^\bullet$	1.20×10^{-20}	29
60	$PQN^\bullet + O_2 \rightarrow PQN + O_2^{\bullet\bullet}$	4.60×10^{-13}	1
61	$PQN^\bullet + O_2^{\bullet\bullet} + 2H^+ \rightarrow PQN + H_2O_2$	3.30×10^{-12}	1
62	$NQN12 + Asch \rightarrow NQN12^\bullet + Asc^\bullet$	1.50×10^{-19}	29
63	$NQN12^\bullet + O_2 \rightarrow NQN12 + O_2^{\bullet\bullet}$	4.60×10^{-13}	1
64	$NQN12^\bullet + O_2^{\bullet\bullet} + 2H^+ \rightarrow NQN12 + H_2O_2$	3.30×10^{-12}	1
65	$NQN14 + Asch \rightarrow NQN14^\bullet + Asc^\bullet$	6.30×10^{-21}	29
66	$NQN14^\bullet + O_2 \rightarrow NQN14 + O_2^{\bullet\bullet}$	4.60×10^{-13}	1
67	$NQN14^\bullet + O_2^{\bullet\bullet} + 2H^+ \rightarrow NQN14 + H_2O_2$	3.30×10^{-12}	1
68	$UA + O_3 \rightarrow Products$	9.60×10^{-17}	57

69	$\text{UA} + \cdot\text{OH} \rightarrow \text{Products} + \text{OH}^-$	1.20×10^{-11}	65
70	$\text{GSH} + \cdot\text{OH} \rightarrow \text{Products} + \text{OH}^-$	1.50×10^{-11}	66
71	$\text{GSSG} + \cdot\text{OH} \rightarrow \text{Products} + \text{OH}^-$	1.50×10^{-11}	Assumed to be the same as R67
72	$\text{Asc}^\bullet + \text{Asc}^\bullet + \text{H}^+ \rightarrow \text{Asch} + \text{DHA}$	5.00×10^{-16}	67
73	$\text{Asch} + \text{O}_2^\bullet + \text{H}^+ \rightarrow \text{Asc}^\bullet + \text{H}_2\text{O}_2$	5.10×10^{-17}	1
74	$\text{Asch} + \text{HO}_2 \rightarrow \text{Asc}^\bullet + \text{H}_2\text{O}_2$	2.65×10^{-17}	68
75	$\text{Asch} + \cdot\text{OH} \rightarrow \text{Products} + \text{OH}^-$	1.80×10^{-11}	69
76	$\text{Asch} + \cdot\text{O}_3 \rightarrow \text{Products}$	9.10×10^{-17}	57
77	$1.25 \text{GS}^- + 0.5 \text{O}_3 \rightarrow \text{Products}$	9.60×10^{-20}	57
78	$1.25 \text{GSH} + 0.5 \text{O}_3 \rightarrow \text{Products}$	9.60×10^{-20}	57
79	$\text{GSOO} + \text{GSOO} \rightarrow 0.56 \text{O}_2^\bullet + \text{Products}$	6.79×10^{-13}	70
80	$\text{O}_2^\bullet + \text{GSH} \rightarrow \text{GSO}^\bullet + \text{OH}^-$	3.32×10^{-19}	71–73
81	$\text{NO}_2^\bullet + \text{GS}^\bullet \rightarrow \text{GSNO}_2$	4.98×10^{-12}	4
82	$\text{GSOO}^\bullet + \text{NO}_2^\bullet \rightarrow \text{GSOONO}_2$	2.49×10^{-12}	70
83	$\text{GSOONO}_2 \rightarrow \text{GSOO}^\bullet + \text{NO}_2^\bullet$	7.5×10^{-1}	70
84	$\text{NO}_2^\bullet + \text{GS}^- \rightarrow \text{NO}_2^- + \text{GS}^\bullet$	4.00×10^{-13}	4
85	$\text{NO}_2^\bullet + \text{GSH} \rightarrow \text{NO}_2^- + \text{GS}^\bullet + \text{H}^+$	1.66×10^{-14}	74
86	$\text{GSOO}^\bullet + \text{GSH} \rightarrow \text{GSO}^\bullet + \text{GSOH}$	3.32×10^{-15}	4
87	$\text{GSO}^\bullet + \text{NO}_2 \rightarrow \text{GSOONO}$	7.47×10^{-12}	4
88	$\text{GSOONO} \rightarrow \text{Products}$	7.00×10^2	4
89	$\text{GS}^\bullet + \text{GS}^- \rightarrow \text{GSSG}^\bullet$	1.59×10^{-14}	4,5
90	$\text{GSSG}^\bullet \rightarrow \text{GS}^\bullet + \text{GS}^-$	1.60×10^5	4,5
91	$\text{GSSG}^\bullet + \text{O}_2 \rightarrow \text{GSSG} + \text{O}_2^\bullet$	8.30×10^{-12}	4,5
92	$\text{GS}^\bullet + \text{GS}^\bullet \rightarrow \text{GSSG}$	8.30×10^{-12}	5
93	$\text{GSOH} + \text{GSH} \rightarrow \text{GSSG} + \text{H}_2\text{O}$	1.20×10^{-18}	75
94	$\text{GSO}^\bullet + \text{GSO}^\bullet \rightarrow \text{Products}$	9.96×10^{-14}	4
95	$\text{GS}^- + \text{H}_2\text{O}_2 \rightarrow \text{GSOH} + \text{OH}^-$	1.60×10^{-21}	75
96	$\text{GS}^\bullet + \text{Asch} \rightarrow \text{GSH} + \text{Asc}^\bullet$	1.00×10^{-12}	76,77
97	$\text{UA} + \text{NO}_2^\bullet \rightarrow \text{UA}^\bullet + \text{NO}_2^-$	3.00×10^{-14}	78,79
98	$\text{AscH} + \text{NO}_2^\bullet \rightarrow \text{Asc}^\bullet + \text{NO}_2^-$	5.80×10^{-14}	78,79
99	$\text{UA}^\bullet + \text{Asch} \rightarrow \text{UA} + \text{Asc}^\bullet$	1.70×10^{-15}	77
100	$\text{GS}^\bullet + \text{UA} \rightarrow \text{GSH} + \text{UA}^\bullet$	5.00×10^{-14}	74
101	$\text{O}_2^\bullet + \text{NO}_2^\bullet \rightarrow \text{O}_2\text{NOOm}$	7.50×10^{-12}	4,80
102	$\text{O}_2\text{NOO}^- \rightarrow \text{NO}_2^- + \text{O}_2$	7.00×10^{-1}	4
103	$\text{O}_2\text{NOO}^- \rightarrow \text{O}_2^\bullet + \text{NO}_2^\bullet$	1.10×10^0	4
104	$\text{NO}_2^\bullet + \text{NO}_2^\bullet \rightarrow \text{N}_2\text{O}_4$	7.50×10^{-13}	81

105	$\text{N}_2\text{O}_4 \rightarrow \text{NO}_2^\bullet + \text{NO}_2^\bullet$	6.90×10^3	81
106	$\text{N}_2\text{O}_4 + \text{H}_2\text{O} \rightarrow \text{NO}_2^- + \text{NO}_3^- + 2\text{H}^+$	1.00×10^3	4
107	$\text{O}_2^- + \text{O}_3 + \text{H}_2\text{O} \rightarrow \cdot\text{OH} + 2\text{O}_2 + \text{OH}^-$	2.50×10^{-12}	82
108	$\text{HO}_2 + \text{O}_3 \rightarrow \cdot\text{OH} + 2\text{O}_2$	1.66×10^{-17}	82
109	$\text{NO}_2^- + \cdot\text{OH} \rightarrow \text{NO}_2^\bullet + \text{OH}^-$	8.80×10^{-12}	80
110	$\cdot\text{OH} + \text{NO}_2^\bullet \rightarrow \text{NO}_3^- + \text{H}^+$	7.50×10^{-12}	4
111	$\cdot\text{OH} + \text{NO}_2^\bullet \rightarrow \text{ONOOH}$	7.50×10^{-12}	4
112	$\text{ONOOH} \rightarrow \text{NO}_2^\bullet + \cdot\text{OH}$	3.00×10^{-1}	4
113	$\text{ONOOH} \rightarrow \text{NO}_3^- + \text{H}^+$	7.00×10^{-1}	4
114	$\text{ONOO}^- + \text{GSH} \rightarrow \text{NO}_2^- + \text{GSOH}$	1.10×10^{-18}	83
115	$\text{GSO}^\bullet + \text{NO}_2^\bullet \rightarrow \text{GSOONO}$	7.50×10^{-12}	4
116	$\text{GSOONO} + \text{H}_2\text{O} \rightarrow \text{Products}$	7.00×10^2	4
117	$\text{ONOOH} + \text{AscH} \rightarrow \text{Im}_1$	1.66×10^{-15}	84
118	$\text{Im}_1 \rightarrow \text{ONOOH} + \text{AscH}$	5.00×10^2	84
119	$\text{Im}_1 \rightarrow \text{Im}_2$	4.00×10^1	84
120	$\text{Im}_2 \rightarrow \text{Im}_1$	5.00×10^0	84
121	$\text{Im}_2 + \text{AscH} \rightarrow \text{Asc} + \text{DHA} + \text{NO}_2^- + \text{H}_2\text{O}$	1.66×10^{-19}	84
122	$\text{Im}_2 \rightarrow \text{Asc} + \text{NO}_3^- + \text{H}^+$	8.50×10^{-1}	84
123	$\text{ONOOH} + \text{UA} \rightarrow \text{UA}^{\text{rad}} + \text{NO}_2 + \text{Products}$	2.60×10^{-19}	85
124	$\text{O}_2^\bullet + \text{SOD} + \text{H}^+ \rightarrow 0.5 \text{ H}_2\text{O}_2 + \text{SOD}$	2.65×10^{-12}	See text S2.
125	$\text{H}_2\text{O}_2 + \text{catalase} \rightarrow \text{H}_2\text{O} + 0.5 \text{ O}_2 + \text{catalase}$	3.20×10^{-14}	See text S2.
126	$\cdot\text{OH} + \text{organic matter} \rightarrow \text{oxidized organic matter}$	1.66×10^{-12}	21,65

Table S2. Input parameters to the KM-SUB-ELF model

Parameter	Description	Value
KH_{ccO_3}	Henrys law equilibrium constant for O_3 [aq]/[gas]	1.7×10^{-1}
KH_{ccNO_2}	Henrys law equilibrium constant for NO_2 [aq]/[gas]	2.2×10^{-1}
KH_{ccNO}	Henrys law equilibrium constant for NO [aq]/[gas]	3.9×10^{-2}
KH_{ccOH}	Henrys law equilibrium constant for OH [aq]/[gas]	4.3×10^2
KH_{ccHO_2}	Henrys law equilibrium constant for HO_2 [aq]/[gas]	1.7×10^3
$KH_{ccH_2O_2}$	Henrys law equilibrium constant for H_2O_2 [aq]/[gas]	9.9×10^4
ω_{O_3}	Mean thermal velocity of O_3	$3.7 \times 10^4 \text{ cm s}^{-1}$
ω_{NO_2}	Mean thermal velocity of NO_2	$3.8 \times 10^4 \text{ cm s}^{-1}$
ω_{NO}	Mean thermal velocity of NO	$4.7 \times 10^4 \text{ cm s}^{-1}$
ω_{OH}	Mean thermal velocity of OH	$6.2 \times 10^4 \text{ cm s}^{-1}$
ω_{HO_2}	Mean thermal velocity of HO_2	$4.5 \times 10^4 \text{ cm s}^{-1}$
$\omega_{H_2O_2}$	Mean thermal velocity of H_2O_2	$4.4 \times 10^4 \text{ cm s}^{-1}$
MW_{aa}	Average molecular weight of amino acids	125 g mole^{-1}
MW_{Cu}	Molecular weight copper	63.6 g mole^{-1}
MW_{Fe}	Molecular weight iron	55.6 g mole^{-1}
MW_{SOA}	Average molecular weight SOA	250 g mole^{-1}
MW_{PQN}	Molecular weight phenanthrenequinone (PQN)	$208.2 \text{ g mole}^{-1}$
MW_{NQN}	Molecular weight naphthoquinone (NQN)	$158.2 \text{ g mole}^{-1}$
$pK_{a_{GSH}}$	Acid dissociation constant of GSH	8.8
$pK_{a_{HO_2}}$	Acid dissociation constant of HO_2	4.8
$pK_{a_{ONOOH}}$	Acid dissociation constant of ONOOH	6.5
VR	Lung ventilation rate	$1.5 \text{ m}^3 \text{ h}^{-1}$
BR	Breathing rate	16 min^{-1}
FCR	Functional residual capacity of the lung	2750 cm^3
TV	Tidal Volume – Breath volume	1500 cm^3
SA_{ELF}	Total ELF surface area	890000 cm^2
T_{RT}	Respiratory tract temperature	37°C
pH_{ELF}	pH of the ELF	7

662 **Table S3.** List of symbols and definitions

Symbol	Meaning	SI unit
C_Y	ELF concentration of PM2.5 constituent Y	$\mu\text{mol L}^{-1}$
$C_{\text{gas,PM2.5}}$	Ambient gas phase concentration of PM2.5	$\mu\text{g m}^{-3}$
$C_{\Sigma\text{ROS}}$	ROS concentration in the ELF during or after model simulation	nmol L^{-1}
$d_{\text{PM2.5}}$	Fraction of PM2.5 that deposits in the ELF	
$D_{\text{PM2.5}}$	Dose of PM2.5 deposited in the ELF	μg
$I_{i\rightarrow j}$	Gross chemical interconversion between individual ROS in the ELF	nmol L^{-1}
$I_{\Sigma\text{ROS}}$	Gross chemical interconversion between all ROS in the ELF	nmol L^{-1}
MF_Y	PM2.5 mass fraction of constituent Y	
M_Y	Molar mass of PM2.5 constituent Y	g mol^{-1}
$N_{\Sigma\text{ROS}}$	Cumulative production of ROS in the ELF	nmol L^{-1}
$N'_{\Sigma\text{ROS}}$	Cumulative production rate of ROS in the ELF	$\text{nmol L}^{-1} \text{ s}^{-1}$
$P_{\Sigma\text{ROS}}$	Gross chemical production of ROS in the ELF	nmol L^{-1}
$P'_{\Sigma\text{ROS}}$	Gross chemical production rate of ROS in the ELF	$\text{nmol L}^{-1} \text{ s}^{-1}$
P	Gross chemical production of an individual ROS in the ELF	nmol L^{-1}
SF_Y	Soluble fraction of PM2.5 constituent Y in ELF	
t_{acc}	Accumulation time of PM2.5 in the ELF	h
t_{sim}	Model simulation time	h
V_{ELF}	Volume of the ELF	mL
VR	Lung ventilation rate	$\text{m}^3 \text{ h}^{-1}$
Y_{OH}	OH yield in the ELF	pmol

663

Table S4. Mathematical formulas used to calculate ELF ROS metrics

$$\begin{aligned} I_{\Sigma\text{ROS}} &= \sum_{j,i>j} I_{i\rightarrow j} \\ N_{\Sigma\text{ROS}} &= P_{\Sigma\text{ROS}} - I_{\Sigma\text{ROS}} \\ N'_{\Sigma\text{ROS}} &= (P_{\Sigma\text{ROS}} - I_{\Sigma\text{ROS}}) / t_{\text{sim}} \\ P'_{\Sigma\text{ROS}} &= P_{\Sigma\text{ROS}} / t_{\text{sim}} \end{aligned}$$

664

Table S5. PM2.5 and transition metal concentrations with mass fractions as quantified in PM2.5 collected at different sampling sites throughout the world.

Sampling location	PM2.5 ($\mu\text{g m}^{-3}$)	Fe (ng m^{-3})	Cu (ng m^{-3})	Fe mass fraction	Cu mass fraction	Reference
Amazon (wet season)	1.65	33	0.07	2.00×10^{-2}	4.24×10^{-5}	86
Mace Head (Ireland)	4.2	5.68	0.71	1.35×10^{-3}	1.69×10^{-4}	87
Amazon (dry season)	4.87	19	0.8	3.90×10^{-3}	1.64×10^{-4}	86
Edinburgh (Scotland)	7.1	27.6	1.39	3.89×10^{-3}	1.96×10^{-4}	88
West Midlands (UK, rural)	7.6	51.3	13.5	6.75×10^{-3}	1.78×10^{-4}	89
West Midlands (UK, urban)	9	80.2	13.9	8.91×10^{-3}	1.54×10^{-3}	89
Skukuza (South Africa)	9.4	51	0.41	5.43×10^{-3}	4.36×10^{-5}	90
Amazon (Serro do Navio)	9.87	120	1.65	1.22×10^{-2}	1.67×10^{-4}	91
Amazon (Cuiabá)	10.5	175	1.55	1.67×10^{-2}	1.48×10^{-4}	91
West Midlands (UK, rural, average)	10.5	87.1	20	8.30×10^{-3}	1.91×10^{-3}	89
West Midlands (UK, urban, average)	11.6	102	21.9	8.79×10^{-3}	1.89×10^{-3}	89
Helsinki (Finland)	11.8	96	3.1	8.14×10^{-3}	2.63×10^{-4}	92
Tampa (Florida)	12.7	79	2.4	6.22×10^{-3}	1.89×10^{-4}	93
Toronto (Canada)	12.7	55	2.5	4.33×10^{-3}	1.97×10^{-4}	94
South Phoenix (Texas)	12.95	147	7.6	1.14×10^{-2}	5.87×10^{-4}	95
Tehran (inside a school dormitory)	14	102.13	22.17	7.30×10^{-3}	1.58×10^{-3}	96
Tehran (inside a retirement home)	15	130.78	25.1	8.72×10^{-3}	1.67×10^{-3}	96
South-Eastern Italy (background sites)	16.4	86.8	3.1	5.29×10^{-3}	1.89×10^{-4}	97
Patras (Greece)	17.4	124	7.28	7.13×10^{-3}	4.18×10^{-4}	98
Yeongwol (South Korea)	19.7	31.2	9.8	1.58×10^{-3}	4.98×10^{-4}	99
Budapest (Hungary)	20	430	18.3	2.15×10^{-2}	9.15×10^{-4}	100
South-Eastern Italy (industrial sites)	21.7	85	5.1	3.92×10^{-3}	2.35×10^{-4}	97

Zabrze (upper Silesia, Poland)	22	160.8	6.5	7.31×10^{-3}	2.96×10^{-4}	101
Chuncheon (South Korea)	23	29.6	9.9	1.29×10^{-3}	4.30×10^{-4}	99
Detroit (Michigan)	23	234	6	1.02×10^{-2}	2.61×10^{-4}	102
Megalopolis (Greece)	23	87	4.02	3.78×10^{-3}	1.75×10^{-4}	98
Tehran (outside a retirement home)	24	238.81	25.99	9.95×10^{-3}	1.08×10^{-3}	96
South-Eastern Italy (urban sites)	24.1	78.8	5.7	3.27×10^{-3}	2.37×10^{-4}	97
Tehran (outside a school dormitory)	26	280	32.42	1.08×10^{-2}	1.25×10^{-3}	96
Anaheim (California)	26.8	29.6	39.6	1.11×10^{-3}	1.48×10^{-3}	103
Milan (Summer, Italy)	27.2	186	10	6.84×10^{-3}	3.68×10^{-4}	104
Jeddah City (Saudi Arabia)	28.4	590	5.6	2.08×10^{-2}	1.97×10^{-4}	105
Hong Kong	29	140	5.7	4.83×10^{-3}	1.97×10^{-4}	106
Rio de Janeiro (Brazil)	29.2	307	35	1.05×10^{-2}	1.20×10^{-3}	107
Katowice (upper Silesia, Poland)	31	157	8.2	5.07×10^{-3}	2.65×10^{-4}	101
Porto Marghera (Italy)	31	200	9.3	6.45×10^{-3}	3.00×10^{-4}	108
Erzgebirge (Germany)	32.5	188	3	5.79×10^{-3}	9.23×10^{-5}	109
Barcelona (Spain)	35	260	52	7.43×10^{-3}	1.49×10^{-3}	110
Santa Catarina (Mexico)	36.15	466	16	1.29×10^{-2}	4.42×10^{-4}	111
Escobedo (Mexico)	37.78	493	13	1.31×10^{-2}	3.44×10^{-4}	111
Arnhem (the Netherlands)	38.95	241	13.5	6.19×10^{-3}	3.47×10^{-4}	112
Mira Loma (Southern California, average)	41.8	581	75	1.39×10^{-2}	1.79×10^{-3}	113
Taif (residential area, Saudi Arabia)	46	2000	5.3	4.35×10^{-2}	1.15×10^{-4}	114
Taif (industrial site, Saudi Arabia)	47	2300	13	4.89×10^{-2}	2.77×10^{-4}	114
Azusa (California)	47.1	281.9	13.4	5.99×10^{-3}	2.85×10^{-4}	103
Edison (New Jersey)	49.6	1953	10	3.94×10^{-2}	2.02×10^{-4}	115
Bursa (Turkey)	53	875	15	1.65×10^{-2}	2.83×10^{-4}	116
Karachi (summer, Pakistan)	55.89	3360	56	6.01×10^{-2}	1.00×10^{-3}	117
New Delhi (summer, high traffic, India)	58.2	710	20	1.22×10^{-2}	3.44×10^{-4}	118

Milan (Winter, Italy)	58.6	309	18	5.27×10^{-3}	3.07×10^{-4}	104
Thessaloniki (cold period, Greece)	60.9	2890	93	4.75×10^{-2}	1.53×10^{-3}	119
Thessaloniki (warm period, Greece)	70.6	4094	66	5.60×10^{-2}	9.35×10^{-4}	119
Córdoba City (Argentina)	70.87	325	8	4.59×10^{-3}	1.13×10^{-4}	120
Shanghai (China)	71.61	424.93	9.47	5.93×10^{-3}	1.32×10^{-4}	121
Yong'an (Winter, China)	79.01	582.1	19.6	7.37×10^{-3}	2.48×10^{-4}	122
Yong'an (Spring, China)	83.26	736.1	16.5	8.84×10^{-3}	1.98×10^{-4}	122
Karachi (winter, Pakistan)	98.44	3706	39	3.77×10^{-2}	3.96×10^{-4}	117
Ji'nan (urban site, China)	101	1040	30	1.03×10^{-2}	2.97×10^{-4}	123
Guangzhou (China)	104.58	66	60	6.31×10^{-4}	5.74×10^{-4}	124
Argra (urban, India)	104.9	1900	200	1.81×10^{-2}	1.91×10^{-3}	125
Pune (India)	113.8	2090	339	1.84×10^{-2}	2.98×10^{-3}	126
Beijing (Summer, China)	125	1060	44.7	8.48×10^{-3}	3.58×10^{-4}	127
Ji'nan (industrial site, China)	130	2410	40	1.85×10^{-2}	3.08×10^{-4}	123
Beijing (Winter, China)	138	1330	53.2	9.64×10^{-3}	3.86×10^{-4}	127
Beijing (China)	182.2	1180	70	6.48×10^{-3}	3.84×10^{-4}	128
New Delhi (winter, high traffic, India)	276.9	1150	70	4.15×10^{-3}	2.53×10^{-4}	118
Peat fire episode (Indonesia)	640	4810	100	7.52×10^{-3}	1.56×10^{-4}	129
<i>Iron and copper medians</i>	—	—	—	8.14×10^{-3}	3.07×10^{-4}	<i>This study</i>

Table S6. PM2.5 and SOA concentrations with mass fractions as quantified in PM2.5 collected at different sampling sites throughout the world.

Sampling location	PM2.5 ($\mu\text{g m}^{-3}$)	SOA ($\mu\text{g m}^{-3}$)	SOA mass fraction	Reference
Amazon (Brazil)	1.8	0.34	0.189	130
Hyytiälä (Finland)	2	1.2	0.60	131
Storm Peak (Colorado)	2.1	0.7	0.333	131

Jungfraujoch (Switzerland)	2.2	1.2	0.545	131
Duke Forest (North Carolina)	2.8	1.3	0.464	131
Chebogue Pt. (Canada)	2.9	1.5	0.517	131
Edinburgh (Scotland)	3	1.2	0.400	131
Mainz (Germany)	4.3	1.1	0.256	131
Boulder (Colorado)	4.4	2.5	0.568	131
Manchester (winter, UK)	5.2	0.6	0.115	131
Chelmsford (UK)	5.3	1.8	0.340	131
Vancouver (Canada)	7	2.5	0.357	131
Okinawa (Japan)	7.9	1.7	0.215	131
Off New England Coast	8.5	4.9	0.576	131
Thompson Farm (New Hampshire)	9.5	4.2	0.442	131
Zurich (winter, Switzerland)	9.6	4.3	0.448	131
Cheju (South Korea)	10.7	4	0.374	131
Fukue (Japan)	11	3.6	0.327	131
New York City (winter, New York)	11.6	2.6	0.224	131
New York City (summer, New York)	12.2	4.8	0.393	131
Pinnacle Park (New York)	12.3	5.4	0.439	131
Houston (Texas)	12.8	2.7	0.211	131
Tokyo (summer, Japan)	13.2	4.7	0.356	131
Manchester (summer, UK)	14.3	3	0.210	131
Pittsburgh (Pennsylvania)	14.7	3.1	0.211	131
Tokyo (winter, Japan)	16.2	2.3	0.142	131
Taunus (Germany)	16.3	7.9	0.485	131
Riverside (California)	19.1	7	0.366	131
Zurich (summer, Switzerland)	25.5	5.1	0.200	131
Mexico City (Mexico)	26.8	8.1	0.302	131

Guangzhou (China)	69.1	12.5	0.181	132
Beijing (China)	79.9	16.6	0.208	132
Shanghai (China)	90.7	11.1	0.122	132
Beijing (China)	158.5	40.9	0.258	132
Xi'an (China)	345.1	53.5	0.155	132
<i>SOA median</i>	—	—	0.333	<i>This study</i>

Table S7. PM2.5, Phenanthrenequinone (PQN), 1,4-naphthoquinone (1,4-NQN) and 1,2-naphthoquinone (1,2-NQN) concentrations with mass fractions as quantified in PM2.5 collected at different sampling sites throughout the world. *see SI section on particulate pollutant concentrations in the ELF.

Sampling location	PM2.5 ($\mu\text{g m}^{-3}$)	PQN (ng m^{-3})	1,2-NQN (ng m^{-3})	1,4-NQN (ng m^{-3})	PQN mass fraction	1,2-NQN mass fraction	1,4-NQN mass fraction	Reference
Umea (Sweden)	7.8	Unknown	Unknown	0.03	2.6×10^{-6}	1.3×10^{-6}	1.3×10^{-6}	133
Athens (Greece)	35.6	0.071	0.157	0.26	2.69×10^{-6}	5.95×10^{-6}	9.86×10^{-6}	134
Mazar-e Sharif (Afghanistan)	69	Unknown	Unknown	0.027	1.06×10^{-6}	5.28×10^{-7}	5.28×10^{-7}	133
Kabul (Afghanistan)	86	Unknown	Unknown	0.2	6.28×10^{-6}	3.14×10^{-6}	3.14×10^{-6}	133
								120
Atascadero (California)	5*	0.023	0.0127	0.0246	6.21×10^{-6}	3.43×10^{-6}	6.64×10^{-6}	
Birmingham (UK)	15*	4.6	3.2	1.7	4.14×10^{-4}	2.88×10^{-4}	1.53×10^{-4}	136
Lake Elsinore (California)	20*	0.311	0.246	0.14	2.1×10^{-5}	1.66×10^{-5}	9.45×10^{-6}	135
Norfolk (UK)	5*	0.058	0.024	0.012	1.57×10^{-5}	6.48×10^{-6}	3.24×10^{-6}	137
Riverside (California)	25*	0.57	0.06	0.23	3.08×10^{-5}	3.24×10^{-6}	1.24×10^{-5}	138
<i>Quinones median</i>	—	—	—	—	6.28×10^{-6}	3.43×10^{-6}	6.64×10^{-6}	<i>This study</i>

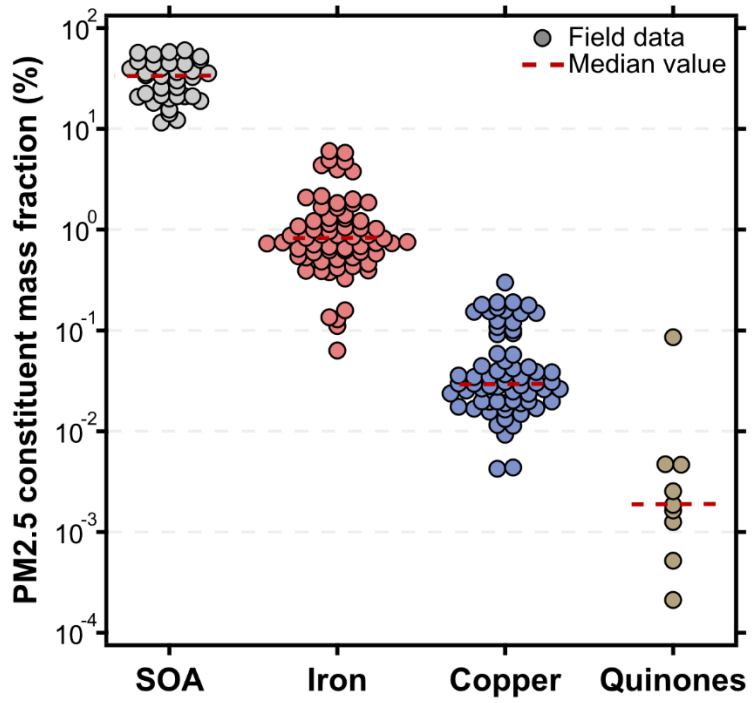


Figure S1. Mass fractions of all redox-active PM2.5 constituents quantified in field data (Tabs. S5-7). The median mass fraction of each redox-active PM2.5 constituent is indicated by the red horizontal line.

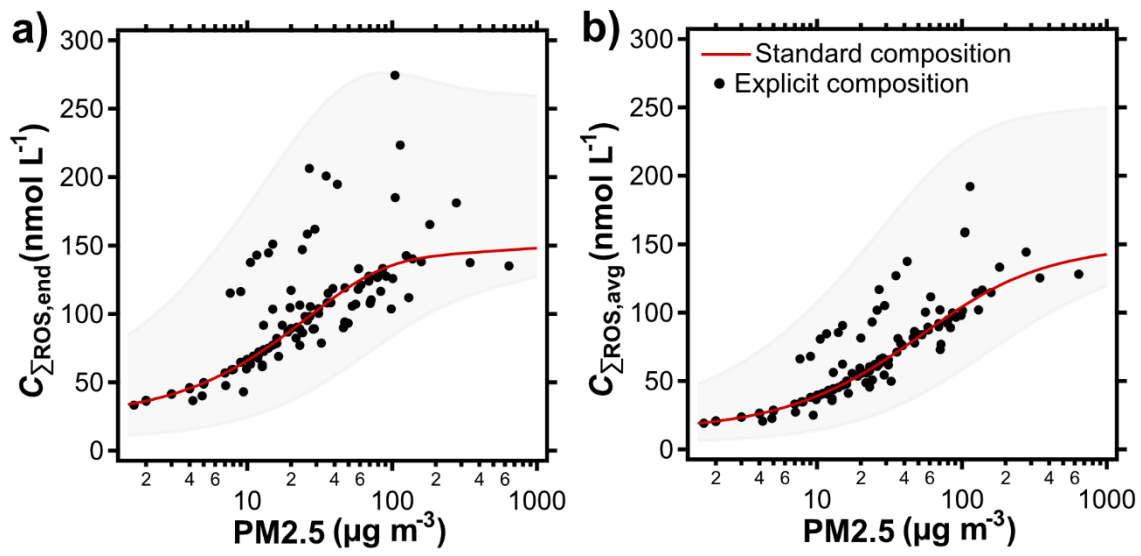


Figure S2. (a) ROS concentration, $C_{\Sigma\text{ROS},\text{end}}$, after pollutant exposure, and (b) the average ROS concentration, $C_{\Sigma\text{ROS},\text{avg}}$, during pollutant exposure as a function of PM2.5 concentration. The solid lines represent a standard composition of PM2.5 using median mass fractions of the redox-active constituents. Black markers represent calculations using explicit PM2.5 composition field data (Tab. S5-7)

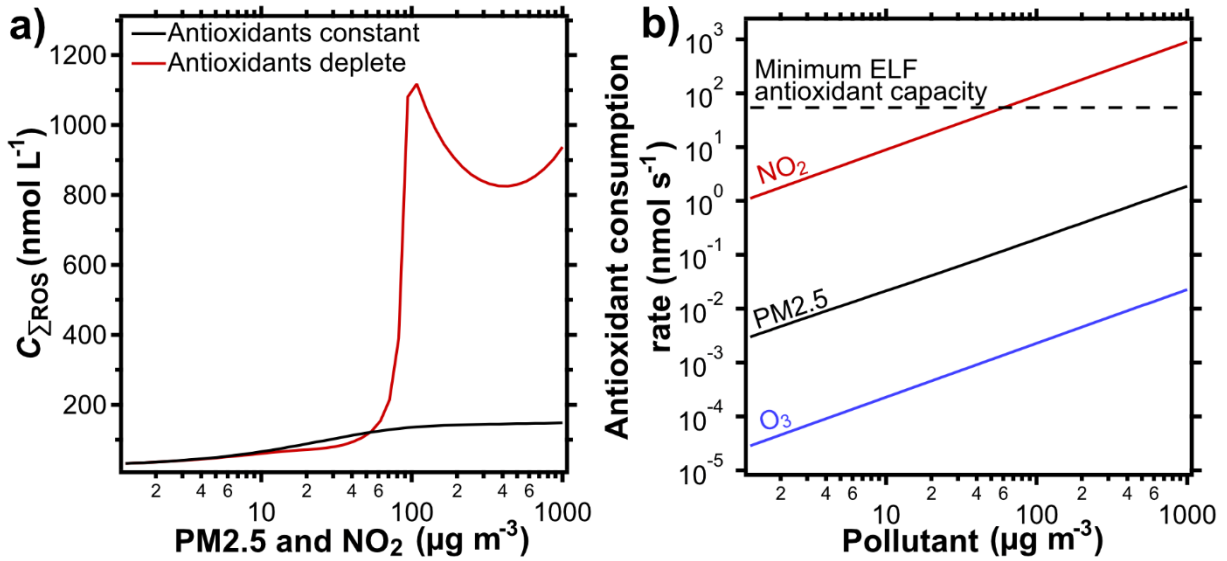


Figure S3. (a) ROS concentrations, $C_{\Sigma\text{ROS}}$, as a function of pollutant concentration with and without consideration of antioxidant depletion in the model. One µg of the co-pollutant NO₂ is added per µg PM2.5. For O₃, a constant concentration of 30 µg m⁻³ was used, independent of PM2.5 concentration. (b) Antioxidant consumption rate of NO₂, PM2.5 and O₃ as a function of pollutant concentration. The dashed line indicates the antioxidant consumption rate at which the ELF antioxidants would deplete in healthy humans within two hours of pollutant exposure without the consideration of enzymes or antioxidant replenishment.

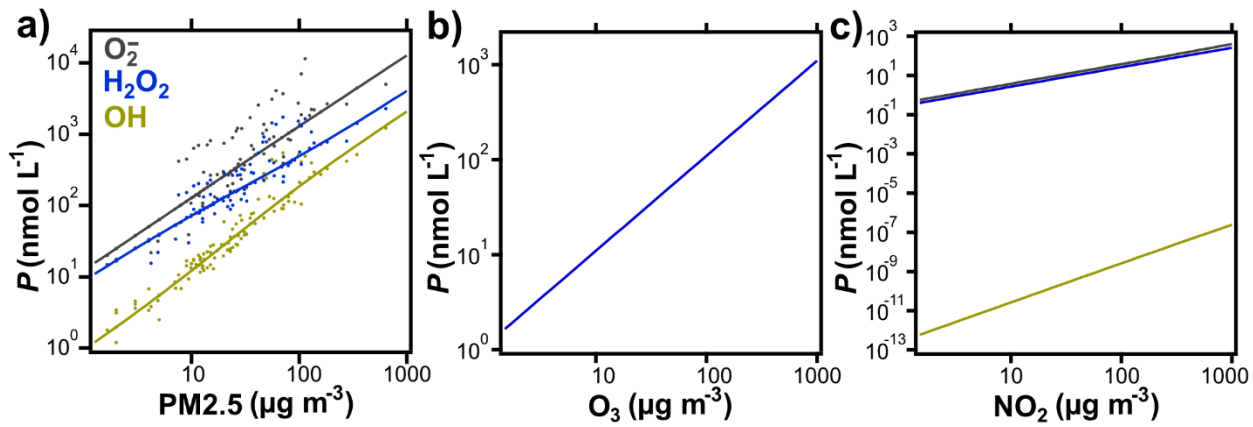


Figure S4. Gross chemical production of individual ROS in the ELF solely associated with and as a function of the concentration of three pollutants: (a) PM2.5, (b) O_3 , and (c) NO_2 . Simulations were carried out using only the single pollutant. In panel a, the solid lines represent standard PM2.5 composition, and the markers represent explicit PM2.5 composition data for redox-active constituents (Tabs. S5-7). O_3 does not contribute to production of O_2^- or OH in the model.

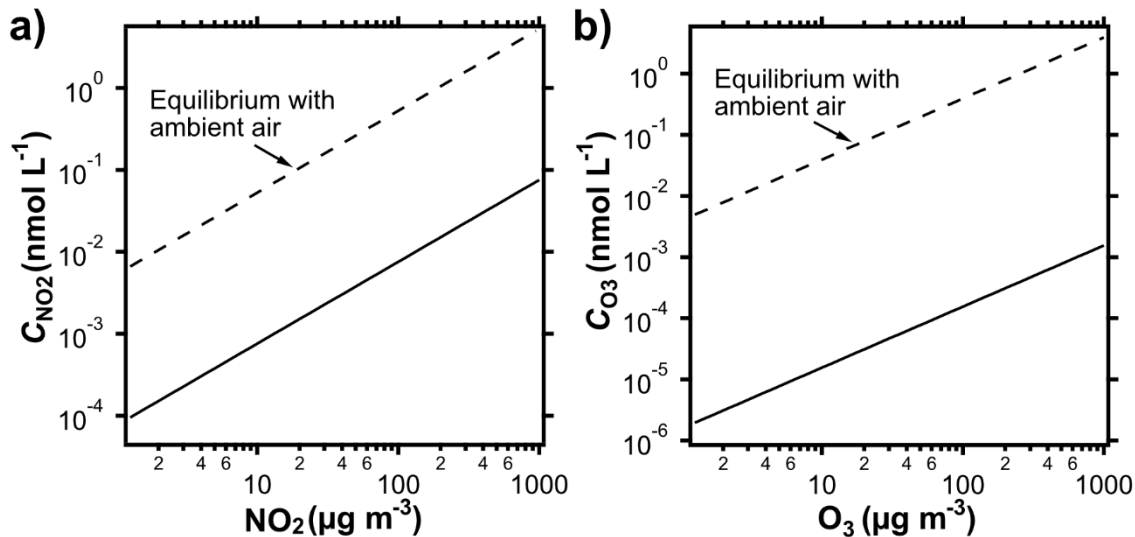


Figure S5. Aqueous-phase (a) NO_2 concentration and (b) O_3 concentration in the ELF as a function of pollutant concentration and comparison to hypothetical saturation with respect to ambient air. Dashed lines indicate saturation concentrations assuming Henry's law equilibrium, which are calculated using the ambient gas phase pollutant concentration and the dimensionless water-air partitioning coefficients for O_3 and NO_2 , respectively (Table S2).

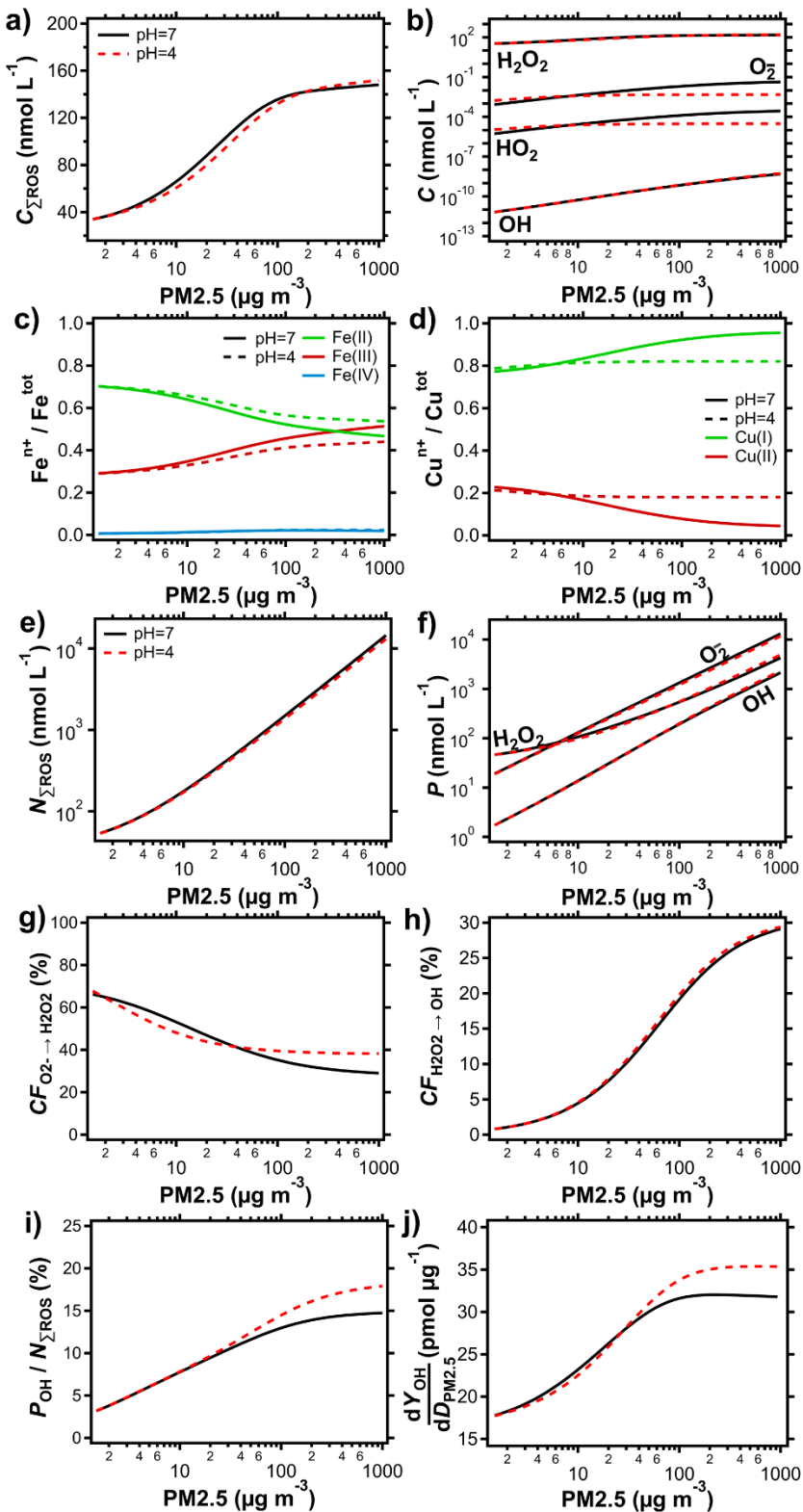


Figure S6. Effect of using different pH on the main results (panels a,b, e-j) and transition metal valence state (panels c,d) using the median mass fractions of all redox-active PM2.5 constituents, co-varied NO_2 ($\text{PM2.5}:\text{NO}_2 = 1:1$) and an O_3 concentration of $30 \mu\text{g m}^{-3}$.